Surface Jumping: Frank Condon factors and Condon points in phase space

S. Kallush[1] Bilha Segev[1] A.V. Sergeev[1]and E.J. Heller[2]

1 *Department of Chemistry, Ben-Gurion University of the Negev, POB 653, Beer-Sheva 84105, ISRAEL*

2 *Departments of Chemistry and Physics, Harvard University, Cambridge, MA 02138 USA*

November 12, 2001

Abstract

We generalize the concept of Tully-Preston surface hopping to include larger *jumps* in the case that the surfaces do not cross. Instead of identifying a complex hopping point, we specify a jump between two locales in phase space. This concept is used here to find propensity rules for the accepting vibrational mode(s) in a radiationless vibronic relaxation transition. A model inspired by the $S_2 \rightarrow S_0$ vibronic relaxation transition of the benzene molecule where 30 modes of vibration compete for the electronic energy is studied within this approach. For this model, we show that almost all the energy must go to a single $C-H$ local stretching. The initial conditions for vibrations of this mode are a coordinate jump of the hydrogen atom toward the ring. All the other modes undergo an almost vertical transition, where the energy that they take is determined by their equilibrium displacement between the two surfaces. We observe that for a large energy gap the masses and frequencies become the defining parameters for choosing the accepting mode. Anharmonicities are very important when a competition between degenerate modes occurs. These conclusions are demonstrated by the specific model considered here but apply in general to any weak internal conversion process.

(Printed November 12, 2001)

1 Introduction

Molecular electronic transitions may be radiative or non-radiative. In either case, the process may be Franck-Condon enhanced or suppressed. The enhanced processes correspond to a crossing of Born-Oppenheimer potential energy surfaces in the classically accessible region, whereas Franck-Condon suppressed events have no such crossing. Examples include radiative processes in the wings of absorption or emission band envelopes, and radiationless events for nested potential energy surfaces.

We focus here on intuition and procedures for realistic polyatomic processes. For the case of surface crossing, the Tully-Preston surface hopping[1] picture has been of considerable value, permitting both intuition and simple procedures for calculating rates of electronic conversion. Some extensions of this approach and insight can be found in Refs. [2, 3].

When the surfaces cross, trajectories can hop smoothly with little or no change in position or momentum at the time of the hop. But often surfaces do not cross. What then? Of course, the rate for such cases is generally lower because of the implied suppression of Franck-Condon factors. However, these suppressed events may be "the only game in town" or may be significant channels competing with others. Analytical continuation is sometimes used in these cases to recognize a complex jumping point in coordinate space [4, 5], and quasiclassical models are also useful [6], but we want a more direct procedure which is applicable to many degrees of freedom. The approach we use is surface jumping[7].

Our paradigm in this paper is a radiationless transition between nested surface potentials as shown in figure 1(b). This situation can also arise radiatively, if we consider say the upper surface to be raised past the absorption maximum by the photon energy $h\nu$ as in figure 1(d). We have in mind a many coordinate example.

Perhaps it is not obvious that any useful classical picture can emerge for this noncrossing situation, since the situation we describe is classically forbidden. However, other classically forbidden processes have very useful classical descriptions, such as barrier tunneling, which involves trajectories in imaginary time or on the inverted potential energy surface.

Recently, some of us have outlined a procedure to recognize the jumping points in phase space in the noncrossing regime [7, 8]. We demonstrated the method by applying it to a two-dimensional harmonic oscillator, a model in which one can find the jumping point analytically [7]. The results were encouraging. Identification of the jumping points was shown to allow for an easy derivation of propensity rules for the distribution of the electronic energy between competing vibrational modes. The treatment was limited in two ways. First, by the assumption of Harmonic potentials and second by the assumption of an allowed transition, with no derivative coupling between the states. Here, we generalize the treatment to transitions between any two multidimensional, non-harmonic potentials and establish the numerical tools that are needed for the recognition of the jumping points in the general case. We also generalize the treatment so that it applies to internal conversion - i.e., electronically forbidden transitions induced by derivative couplings, and study what is then the contribution of the promoting mode.

Questions that we address in this paper are:

- Where will the jump between the two surfaces take place?
- What is the best system of coordinates to describe the process?
- What is the sensitivity of these predictions to the value of various parameters?

The importance of the absolute value of the frequency and the reduced mass of a mode in the determination of its propensity as an accepting mode was previously discussed [9, 10] with implications for the isotope effect for nonradiative decay [10]. Here we supplement these early studies by considering the transition in phase space.

As an example, we apply our approach to a model inspired by a complex physical system, the 30 modes problem of the $S_2 \rightarrow S_0$ transition of the benzene molecule. As detailed below the model imitates some properties of the benzene molecule yet differ from it in some other features. While it is not a complete description of the benzene molecule, much can be learned from it nevertheless. Even for this simplified model of the $S_2 \rightarrow S_0$ transition it is not trivial to determine which modes or combination of the 30 vibrational modes of our system would be first excited during the quantum jump. With the new surface-jumping approach we are able to do so with relative ease.

The outline of the paper is as follows: Surface jumping is defined and analyzed in section II. In section III we apply the method to a model of an $S_2 \rightarrow S_0$ transition inspired by the benzene molecule and study the sensitivity of the results to different conjectures regarding the surface potentials. Section IV concludes and summarizes.

2 Frank-Condon factors in phase space

2.1 Quantum-mechanical treatment in coordinate space

The probability for an allowed transition from the vibronic state i to a vibronic manifold j, where i, j refer to electronic states is given by:

$$P^{i\rightarrow j} = |\mu_{elec}|^2 \sum_{\{n'_k\}} \prod_k \left| \left\langle \chi^j_{n'_k} | \chi^i_{n_k} \right\rangle \right|^2 , \tag{1}$$

Here $\mu_{elec} = \int \psi^*_j \hat{\mu}_{elec} \psi_i d\,\vec{r}$, is the dipole transition moment between the electronic states ψ_i and ψ_j and $\hat{\mu}_{elec}$ is the dipole moment operator. The integration $d\vec{r}$ is over all the electronic coordinates $\vec{r}$. The nuclear wave function for the mode q_k in the electronic state i for vibrationally excited state n_k is $\chi^i_{n_k}$, and separability is assumed. Separability is not necessary for our approach, and we do not use it below for the final state, but here we use it for simplicity. The term $\prod_k \left| \left\langle \chi^j_{n'_k} | \chi^i_{n_k} \right\rangle \right|^2$ in this expression is the

FC factor squared between two vibronic states. The summation, $\sum_{\{n'_k\}}$, is over a manifold of vibronic states, whose energy is equal to the energy of the initial state i. Note that an excited initial state, as considered here, has a finite energy width allowing for many final states with slightly different energies. For internal conversion, an electronically forbidden transition, $\mu_{elec} = 0$ at the equilibrium position. Nevertheless, the transition can occur by nonadiabatic coupling via the kinetic energy operator. The probability for internal conversion from the vibronic state i to another vibronic manifold j is:

$$P^{i\to j} = \sum_{\mathsf{p}} |M^{\mathsf{p}}_{elec}|^2 \sum_{n'_{\mathsf{p}}} \left| \left\langle \chi^j_{n'_{\mathsf{p}}} | \frac{\partial}{\partial q_{\mathsf{p}}} | \chi^i_{n_{\mathsf{p}}} \right\rangle \right|^2 \sum_{\{n'_k \neq n'_p\}} \prod_{k\neq \mathsf{p}} \left| \left\langle \chi^j_{n'_k} | \chi^i_{n'_k} \right\rangle \right|^2 . \tag{2}$$

Here, $M_{elec} = \left\langle \psi^j | \frac{\partial}{\partial q_{\mathsf{p}}} | \psi^i \right\rangle$ is the non-adiabatic interaction matrix element while p serves as the promoting vibration of the normal mode q_{p}. The promoting mode is the mode which couples between the electronic surfaces via its kinetic energy operator and therefore should have the correct symmetry to prevent the electronic matrix element M_e from vanishing. The sum over p takes into account all possible promoting modes. The last term in Eq. (2) is the FC factor squared for the nuclei subspace which includes all the nuclei coordinates except for the one which serves as the promoting mode with a summation over all the possible divisions of the vibrational energy between the modes. In both these cases, the FC factors strongly influence the transition probability and practically control the distribution of the electronic energy that is released in the relaxation process between the competing vibrational modes. It is useful to define the total FC factor squared as:

$$\Sigma_{I\to F} = \sum_{\{n'_k\}} \prod_k \left| \left\langle \chi^j_{n'_k} | \chi^i_{n_k} \right\rangle \right|^2 \tag{3}$$

for an allowed transitions and:

$$\Sigma_{I\to F} = \sum_{n'_{\mathsf{p}}} \left| \left\langle \chi^j_{n'_{\mathsf{p}}} | \frac{\partial}{\partial q_{\mathsf{p}}} | \chi^i_{n_{\mathsf{p}}} \right\rangle \right|^2 \sum_{\{n'_k \neq n'_{\mathsf{p}}\}} \prod_{k\neq \mathsf{p}} \left| \left\langle \chi^j_{n'_k} | \chi^i_{n_k} \right\rangle \right|^2 \tag{4}$$

for internal conversion. Eqs. (3) and (4) were explicitly written for separable states. Generalization to non-separable states is straightforward as applied below.

The rate of the transition is given by Fermi golden rule:

$$\Gamma = \frac{2\pi\kappa^2}{\hbar} \rho_{final} \Sigma_{I\to F} \tag{5}$$

where ρ_{final} is the density of states on the ground electronic state (accepting surface) and κ^2 is the electronic part of either Eq. (1) or (2) for allowed transitions or internal conversion, respectively. This rate can be written as the trace over two density matrixes: $\Gamma = \mathrm{Tr}\left[\hat{\rho}_f \hat{\rho}_i\right]\ 2\pi\kappa^2/\hbar$ for allowed transitions and $\Gamma = \mathrm{Tr}\left[\hat{\rho}_f \hat{\rho}'_i\right]\ 2\pi\kappa^2/\hbar$ for internal conversion, where

$$\hat{\rho}_i = \prod_k |\chi^i_{n_k}\rangle\langle\chi^i_{n_k}|, \tag{6}$$

ρ'_i is defined below, and

$$\hat{\rho}_F = \sum_{\{n'_k\}} \prod_k |\chi^j_{n'_k}\rangle\langle\chi^j_{n'_k}|\ \rho_{final} = \delta\left(\hat{H}_F - E\right), \tag{7}$$

where $\hat{H}_F$ is the Hamiltonian operator of the final electronic surface.

The common way to determine which are the vibrations that are most likely to be excited is to calculate the different FC factors for all possible combinations of different divisions of the energy quanta between the modes [11]. This, however, would demand an enormous computational effort and can

be regarded as impossible for large molecules especially when the energy that is transferred between the degrees of freedom is large. Efficient ways to calculate FC factors are limited to the harmonic approximation [12]. Moreover, when the potential energy surface cannot be treated as separable, the eigenstates themselves are of mixed character and many will share roughly the same FC intensity, without revealing the mechanism or geometry of the jump between surfaces. Indeed, this can happen even for separable surfaces, in that many different final state FC factors could be comparable in size, reflecting the fact that the "jump" was not along any one of the separable coordinates.

2.2 Quantum-mechanical treatment in phase space

Our approach to overcome the difficulties presented in the previous section is to consider the transition in phase space. The donor state is represented by its Wigner function, the acceptor state by a classical energy hypersurface in phase space, and the transition itself is determined by the overlap between the two.

In the Wigner representation the total FC factors squared, multiplied by the final density of states, are expressed as an overlap *integral* in phase space. Our method for the derivation of propensity rules is based on recognizing the points in phase-space in which the FC *integrand* peaks. For weak transitions the integrand that we study tends to be exponentially small, and the dominant region in phase space where this integrand peaks may often be exponentially dominant over the rest of the integral. For convenience, we use an abridged form (q,p) for the nuclear positions and momenta for the set of normal modes $(\{q_k\},\{p_k\})$. In the Wigner phase space representation Γ takes the form:

$$\Gamma = \frac{2\pi\kappa^2}{\hbar}\int_{-\infty}^{\infty} dq \int_{-\infty}^{\infty} dp\ \rho_F(q,p)\ \rho_I(q,p), \tag{8}$$

for allowed transition. Here $\rho_I(q,p)$ and $\rho_F(q,p)$ are the Wigner functions of the initial and final states density matrices $\hat{\rho}_I$ and $\hat{\rho}_F$, respectively, defined in the usual way:

$$\rho(q,p) \equiv \frac{1}{2\pi\hbar}\int_{-\infty}^{\infty} d\eta \left\langle q+\frac{\eta}{2}|\hat{\rho}|q-\frac{\eta}{2}\right\rangle e^{-ip\eta/\hbar}. \tag{9}$$

Practically, we start with the description where each of the *initial* vibrational wave functions for each of the vibrational modes is characterizes by its quasi-distribution, i.e. we assume a separable system, for the excited electronic state. Consequently, the Wigner function $\rho_I(q,p)$ is a simple product of these well defined one dimensional quasi-distributions:

$$\rho_I(q,p) = \prod_k \rho_I^k(q_k,p_k)\,. \tag{10}$$

For internal conversion:

$$\Gamma = \sum_{\mathsf{p}} \Gamma_{\mathsf{p}}\,, \tag{11}$$

$$\Gamma_{\mathsf{p}} = \frac{2\pi\kappa^2}{\hbar}\int_{\infty}^{\infty} dq \int_{\infty}^{\infty} dp\ \rho_F(q,p)\ \rho_I^{(\mathsf{p})\prime}(q,p), \tag{12}$$

where the sum is over the promoting modes,

$$\rho_I^{(\mathsf{p})\prime}(q,p) \equiv \rho_I'^{\mathsf{p}}(q_{\mathsf{p}},p_{\mathsf{p}})\prod_{k\neq\mathsf{p}}\rho_I^k(q_k,p_k)\,, \tag{13}$$

$$\rho_I'^{\mathsf{p}}(q_{\mathsf{p}},p_{\mathsf{p}}) \equiv \left[\hat{\rho}_I'^{\mathsf{p}}\right]_W = \left[\left|\frac{\partial\chi^i_{n_{\mathsf{p}}}}{\partial q_{\mathsf{p}}}\right\rangle\left\langle\frac{\partial\chi^i_{n_{\mathsf{p}}}}{\partial q_{\mathsf{p}}}\right|\right]_W, \tag{14}$$

and $[A]_W$ stands for the Wigner transform of A.

For the *final* state Wigner function, $\rho_F(q,p)$, a formal expression is obtained which substantially simplifies the calculation. For relaxation processes the final state (usually a quasi-continuum manifold

of states) is defined by energy conservation to be given by the density matrix $\delta\left(\hat{H}_F - E\right)$. We define $\Delta(q,p)$ to be the Wigner transform of this Delta-function density and get

$$\Gamma = \frac{2\pi\kappa^2}{\hbar}\int dq\ dp\ \Delta(q,p)\rho_I(q,p), \tag{15}$$

for an allowed transition and

$$\Gamma_{\mathsf{p}} = \frac{2\pi\kappa^2}{\hbar}\sum_p \int dq\ dp\ \Delta(q,p)\rho_I^{(p)\prime}(q,p), \tag{16}$$

for internal conversion.

In our search for the direction of the surface jump we look for the point(s) or region(s) in phase-space (q^*,p^*) where the integrand, $\Delta(q,p)\rho_I(q,p)$, or $\Delta(q,p)\rho_I^{(\mathsf{p})'}(q,p)$, peaks.

2.3 Surface jumping

The Wigner function of the quasi-continuum final state $\Delta(q,p)$ can be expanded as an asymptotic power series in $\hbar$ [13, 14, 15, 16]. A criterion for the validity of the asymptotic series expansion is given by:

$$\left(\frac{\hbar^2}{2m\,|\nabla V|}\right)^{1/3} < \sigma \tag{17}$$

where σ is the width of the initial wave function on the excited electronic surface, m is the reduced mass of the oscillator and $|\nabla V|$ is the magnitude of the gradient of the surface potential at the point of the transition. The zero order of this expansion which is in some sense a semiclassical approximation gives:

$$\Delta(q,p) \to \delta[E - H_F(q,p)] \tag{18}$$

where H_F is the classical Hamiltonian for the final (accepting) electronic state. Expansion to order $\hbar^2$ gives an Airy function instead of the delta function. An *exact* calculation of transition probabilities and rates may require more care, but the relative order of magnitudes of competing transitions as well as the partition of energy between competing accepting modes can be determined already at this semiclassical approximation level [17].

We are looking for the phase-space point(s) (q^*,p^*) where the integrand:

$$\delta[E - H_F(q,p)]\rho_I(q,p) \tag{19}$$

is maximal, i.e. we maximize the initial Wigner function $\rho_I(q,p)$ under the constraint $E = H_F(q,p)$. (For internal conversion $\rho_I(q,p)$ is replaced by $\rho_I^{(p)\prime}(q,p)$ throughout this analysis). The location of these points in phase-space gives us the phase-space jumping point(s) and from it we deduce the accepting modes and an estimation for the energy distribution between competing modes. The value of $\rho_I(q,p)$ at these points indicates to the expected strength of the transition, although we emphasize again that predictions for absolute transition rates must be based on calculation of the *integral* and the electronic prefactors; here, we are finding the dominant pathway for radiationless transition.

The geometric interpretation of the problem is demonstrated in figure 2. The solid inner ellipses represent the contours of the Wigner function, here a gaussian, in some two dimensional space. The outer dashed curve is the energy surface constraint $H_F = E$. The geometric assignment is to find the points where the highest contour of the surface $\rho_I(q,p)$ meets the constraint hypersurface $E = H_F(q,p)$. As demonstrated in figure 2 the strength of the extremal points can vary. Panel (a) shows the case where the point of maximum of the Wigner function under the energy constraint is a *strong maximum*. In this case, there is a very rapid decrease of the Wigner function as one moves away from the extremum point on the energy constraint hypersurface. We can refer to the point as a *true* jumping point. Panel (b) stands as an example for a *weak* extremum. In this diagram the Wigner function contour and the energy constraint hypersurface have a very similar curvature. A decisive jumping point is not well defined.

2.4 Numerical considerations

The identification of the jumping point reduces in this formalism to the mathematical problem of finding the maximum of a multidimensional nonlinear objective function under a nonlinear constraint. Simple geometric considerations show that at all the extremum points the contours of constant initial Wigner function are tangent to the constraint hypersurface:

$$\nabla H_F = \lambda \nabla \rho_I \ . \tag{20}$$

This condition gives a simple set of coupled algebraic equations whose roots define the local extrema. Note that direct multidimensional local minimum finding can be converted by various computational methods (like steepest decent) to a one-dimensional search. It is considered therefore to be a much easier computational problem than a multidimensional root search of a system of non-linear equations [18]. However, numerical methods for local minima finding under a constraint appear to have difficulties in distinguishing between local minima, maxima, and saddle points. We therefore analyze the transition in two steps. We first use a code that takes the Wigner function and the ground electronic surface potential and uses a standard routine to find extremum points (q^*, p^*) of the Wigner function under the energy constraint, and the value of the Wigner function, $\rho_I(q^*, p^*)$, at these points. We then study the Wigner function on the constrained hypersurface at the vicinity of these points using algebraic considerations. The eigenvalues of a tensor of second derivatives in the subspace of the constrained phase space are calculated and the nature of each extremal point, be it a minimum, maximum, or saddle point is determined. For some cases, especially in the harmonic approximation, the problem is also solvable analytically [7].

3 Application to a 30 dimensional model of internal conversion

The model considered here is motivated by the $S_2 \rightarrow S_0$ transition in the benzene molecule [19, 20, 21, 22, 23, 24, 25, 26, 27]. There are theoretical and experimental indications that the benzene molecule is highly distorted on the S_2 surface and that this transition occurs via conical intersections between S_2 and S_1 and between S_1 and S_0, in particular when the initial conditions for the relaxation are a vibrationally excited state on S_2 [28, 26, 27, 29, 30]. We consider a non radiative transition from the vibrationless state of an S_2 electronic term to a manifold of quasi-continuum states of the $S_0(A_{1g})$ ground electronic state. In a future work we will look at the competition between two tunneling mechanisms: that which is responsible for surface jumping considered here and that which accounts for the barrier penetration required to arrive at the conical intersection from a vibrationless initial state on the excited electronic surface. Here we construct our model with no conical intersections. In the rest of the paper, after presenting the model, we find the jumping point for the transition, each time with a different conjecture for the potential energy surfaces (PES). In this way we learn on the possible influences on the jump of different unknown parameters.

3.1 The model

The following properties of benzene are imitated by our model:

- It has one aromatic ring of six carbons and six hydrogens.
- The configuration of the ground S_0 electronic state is hexagonal and belongs to the D_{6h} symmetry group.
- The molecule has 30 modes of vibrations which we number according to Wilson [31]). Some details are given below.
- The vertical energy gap between the S_0 and S_2 state is 0.228 e.V.[32].
- The ground-state potential energy surface is taken from [33]. See below.

- The equilibrium position at S_0 is $q_1^g = 6.47$ Bohrs, $q_2^g = 5.02$ Bohrs and $q_i = 0$ for all other normal modes, by symmetry.
- The equilibrium position at S_2 is sometimes considered as free parameters and sometimes taken as in S_1: $q_1^g = 6.63$ Bohrs and $q_2^g = 5.01$ Bohrs [32].
- Harmonic frequencies on S_2 are taken from [34].

Our model differ from benzene by the following properties:

- The model includes no conical intersections.
- The transition is assumed to be a direct transition from S_2 to S_0 not going through S_1.
- The model assumes a planar molecule on the S_2 surface.

Normal modes which have special importance in the rest of the paper are depicted in Figure 3. Six in plane $C-H$ stretching are each an orthogonal linear combinations of the six local $C-H$ in-plane stretching modes s_i:

$$\begin{pmatrix} q_2\,(a_{1g}) \\ q_7\,(e_{2g}) \\ q_{13}\,(b_{1u}) \\ q_{20}\,(e_{1u}) \\ q_{7a}\,(e_{2g}) \\ q_{20a}\,(e_{1u}) \end{pmatrix} = \frac{1}{\sqrt{6}} \begin{pmatrix} 1 & 1 & 1 & 1 & 1 & 1 \\ \sqrt{2} & -\frac{1}{\sqrt{2}} & -\frac{1}{\sqrt{2}} & \sqrt{2} & -\frac{1}{\sqrt{2}} & -\frac{1}{\sqrt{2}} \\ 1 & -1 & 1 & -1 & 1 & -1 \\ \sqrt{2} & \frac{1}{\sqrt{2}} & -\frac{1}{\sqrt{2}} & -\sqrt{2} & -\frac{1}{\sqrt{2}} & +\frac{1}{\sqrt{2}} \\ 0 & \frac{\sqrt{6}}{2} & -\frac{\sqrt{6}}{2} & 0 & \frac{\sqrt{6}}{2} & -\frac{\sqrt{6}}{2} \\ 0 & \frac{\sqrt{6}}{2} & \frac{\sqrt{6}}{2} & 0 & -\frac{\sqrt{6}}{2} & -\frac{\sqrt{6}}{2} \end{pmatrix} \begin{pmatrix} s_1 \\ s_2 \\ s_3 \\ s_4 \\ s_5 \\ s_6 \end{pmatrix} \tag{21}$$

We take the form of the ground-state potential energy surface from [35] to be:

$$V(\vec{q}) = \frac{1}{2} \sum_{k=1,2} m_k \left(\omega_k^g\right)^2 (q_k - q_k^g)^2 + \frac{1}{6} \sum_{ijk=1,2} \phi_{ijk} r_i r_j r_k + O(q^4) \ , \tag{22}$$

where:

$$r_i = \sqrt{\omega_i^g m_i}(q_i - q_i^g) \tag{23}$$

Here $\omega_k^g = \tilde{\omega}_k^g[cm^{-1}] \,/\, 2R_\infty$, $q_k^g = \tilde{q}_k^g[cm] \,/\, a_0$, and $m_k = \tilde{m}_k \,/\, m_e$, are the frequencies, displacements, and reduced mass of the modes in a.u., where R_∞, a_0, and m_e are Rydberg constant, the Bohr radius, and the electron mass of the ground electronic state respectively. From here on we use the parameters in the a.u. scale. The anharmonic force field constants $\phi_{ijk} = \tilde{\phi}_{ijk}[cm^{-1}] \,/\, 2R_\infty$ are taken from[33].

3.2 An harmonic approximation for both PES

Taking the initial state of S_2 to be the ground state wave function for the normal mode k of a harmonic oscillator we have:

$$\phi_I^k(q_k) = \left(\frac{m_k \omega_k^e}{\pi\hbar}\right)^{1/4} \exp\left[-\frac{1}{2}\frac{m_k \omega_k^e}{\hbar}(q_k - q_k^e)^2\right] \ , \tag{24}$$

where ω_k^e and q_k^e are the frequency and the equilibrium configuration of the k normal mode of the e excited electronic state, respectively. For S_2, $e = 2$. The total wave function is a product of the wave functions of each of the modes. The Wigner transform of a gaussian wave function is another gaussian, for mode k :

$$\rho_I^k(q_k, p_k) = \frac{1}{\pi\hbar} \exp\left[-\frac{m_k \omega_k^e}{\hbar}(q_k - q_k^e)^2 - \frac{p_k^2}{m_k \omega_k^e \hbar}\right] . \tag{25}$$

The initial total Wigner function is:

$$\rho_I(q,p) = \prod_{k=1}^{30} \rho_I^k(q_k, p_k) \equiv \left(\frac{1}{\pi\hbar}\right)^{30} e^{-W}. \tag{26}$$

The $S_2 \rightarrow S_0$ is a forbidden transition. Therefore, when calculating the transition rates or the jumping point, the initial Wigner function $\rho_I(q,p)$ should be replaced by $\rho_I^{(\mathsf{p})\prime}(q,p)$ as defined and explained in section 2.2. Taking ϕ_I^{p} to be as in Eq. (24) we get:

$$\rho_I^{(\mathsf{p})\prime}(q,p) = \frac{m_{\mathsf{p}}\omega_{\mathsf{p}}^e}{\hbar}\left(\frac{m_{\mathsf{p}}\omega_{\mathsf{p}}^e}{\hbar}(q_{\mathsf{p}}-q_{\mathsf{p}}^e)^2 + \frac{p_{\mathsf{p}}^2}{m_{\mathsf{p}}\omega_{\mathsf{p}}^e\hbar}\right)\rho_I(q,p). \tag{27}$$

The integral over the nuclear degrees of freedom giving the transition strength for internal conversion differs from the FC factor squared for an allowed transition by an additional polynomial in the integrand multiplying the Gaussian initial Wigner function. With this additional factor, the transition probability would vanish for a zero excitation of the promoting mode and therefore the promoting mode must have, at least, some minimal excitation.

The jumping point for an allowed transition is found by maximizing $\rho_I(q,p)$ while the jumping point for internal conversion is found by maximizing $\rho_I^{\prime(\mathsf{p})}(q,p)$, both under the same constraint: $H_F(q,p) = E$. It can be shown that when surface jumping occurs these two procedures give the same quantum jump. For large excitations of the promoting mode, the behavior of the Wigner function is dominated by the exponent and the influence of the polynomial is negligible. For small excitations of the promoting mode there is, as mentioned above, a minimal amount of energy that must be transferred to the promoting mode of vibration yet this hardly affects the quantum jump. Thus, we maximize $\rho_I(q,p)$ and not $\rho_I^{(\mathsf{p})\prime}(q,p)$. Therefore, we look for minima of W defined in Eq. (26) under the constraint $H_F(q,p) = E$.

We first consider a harmonic approximation for the Hamiltonian of the lower electronic surface:

$$H_F^h = \frac{1}{2}\sum_{k=1}^{30}\left[\frac{p_k^2}{m_k} + m_k\left(\omega_k^g\right)^2(q_k - q_k^g)^2\right] \ . \tag{28}$$

Results of our calculations show that the extremum points (q^*,p^*) of W under the constraint $H_F^h = E$ form an 11 dimensional subspace within the 60-dimensional phase space of the problem. All of the points in this subspace include a small position excitation of the $C-C$ totally symmetric mode (around 2% of the total energy) and an arbitrary position or momentum excitation of the six $C-H$ in plane stretching modes. The Wigner function $\rho_I(q,p)$ is highly peaked on this subspace with all the points having the same value of the (argument of the) Wigner function, which is our measure of the level of propensity for a transition at these points, $W \cong 32$. Second inspection of the $C-H$ normal modes with the same high propensity show that they have almost the same value of $m_i\omega_i^2$ and could be considered as degenerate oscillators. We conclude that:

- Within a harmonic approximation the surface jumping is restricted to an 11-dimensional hypersurface within the 60-dimensional phase-space of the problem. The surface, with $W \cong 32$, represents all the combinations of in-plane $C-H$ stretching modes subject to the demand of energy conservation.

3.3 Harmonic excited PES and anharmonic ground electronic potential

In this subsection we repeat the analysis of the previous subsection with the same initial harmonic state on the excited electronic surface but this time with the most recent anharmonic force field for the ground state potential surface:

$$H_F = \frac{1}{2}\sum_{k=1}^{30}\left[\frac{p_k^2}{m_k} + m_k\left(\omega_k^g\right)^2(q_k - q_k^g)^2\right] + \frac{1}{6}\sum_{ijk}\phi_{ijk}r_ir_jr_k \ . \tag{29}$$

Although adding the anharmonic force field in this asymmetric fashion does not seem self consistent, we do so first, and then, in a following subsection, we check the possible effects of anharmonicities of the excited surface.

In table 1 we show the points found by the numerical minimization of W under the constraint $H_F = E$. The points which have the lowest value of W, highest propensity, have an almost sixfold

degeneracy with $W \cong 17$. These points correspond to the same small position excitation of the totally symmetric $C-C$ stretching mode and different specific combinations of the six $C-H$ stretching modes position excitations.

The data in the literature led us to perform the analysis in the normal modes of vibrations framework, yet, in order to decode the meaning of the points we have transformed the coordinates from normal modes to local modes using the inverse matrix of the transformation (21). In table 2 we present the same points as in table 1 in local mode coordinates. The physical meaning of the points is now obvious. The six points with the highest propensity refer to six equal points of local mode excitation of $C-H$ stretching with an addition of a very small excitation of the totally symmetric $C-C$ stretching mode which is the only significantly displaced mode within the 30 modes of the benzene.

3.4 Local vs. normal coordinates

The best choice of coordinates for the description of molecular spectroscopy depends on the exact process that has to be described. Low energy vibrational excitations like IR absorption spectroscopy are usually described in terms of normal modes oscillators while high energy processes like dissociation are best described within a local mode framework. It is clear that dissociation of a molecule occurs by breaking one local mode between two atoms; this is inconveniently described by high excitation of several bonds between atoms in the normal mode description.

In our analysis the excitation of a local $C-H$ mode seems to have its origin in the structure of the surface potential. Using the local coordinates, the surface potential for the six in plane $C-H$ stretching modes has the form:

$$V = \sum_{i,j} V_{ij} s_i s_j + \sum_{i,j,k} V_{ijk} s_i s_j s_k \,. \tag{30}$$

Because of the symmetry of the problem $V_{11} = V_{22} = V_{ii}$, $V_{12} = V_{23} = V_{34} = V_{i,i+1}$ etc.. The use of this form reduces the number of parameters that determine the third order anharmonic surface potential to only twelve parameters (instead of 56 in the general normal description). This fact may encourage the attempt to represent the surface potential we took from [33] in local modes. After this transformation of the coordinates we have found that all the cross coefficients in the local modes formulation are very close to zero. We thus find that the potential represents six *separable* anharmonic oscillators. This reduces the number of parameters that describe the anharmonic potential to only *two*. The separability of the potential leads to a straightforward understanding of the reason for a local excitation found in our calculations. It can be proven that in this case of separate potentials with cubic anharmonicity the point with highest propensity corresponds to a single local excitation. We must note here also that the possibility of diagonalizing the potential in local modes was suggested already 30 years ago in order to understand the overtones of the $C-H$ in plane stretching in the IR spectrum of the benzene [36, 37]. A recent treatment of empirical force constants in benzene using local modes for CH stretching was given in Ref. [38]. Here we started with normal modes but are forced by the results of our calculation to change to local modes.

We summarize our conclusions so far:

- Inclusion of anharmonic effects for the ground electronic state reduces the dimensionality of the transition from an 11 dimensional hyperspace to small regions surrounding six degenerate points.
- The points with the highest propensity describe a single excitation of a local mode of $C-H$ stretching and another considerably smaller simultaneous excitation of the totally symmetric $C-C$ stretching mode.

3.5 Influence of the energy gap between the two surfaces

How does the result for the jumping point vary as a function of the energy gap? Figure 4 plots the excitations in the different directions and the value of the Wigner function at the jumping point on the point with the highest propensity versus the energy gap between the states Other parameters like the displacements between the modes are kept fixed. The only mode which changes its excitation due to the change of the energy gap is the mode which undergoes the jump, here - local $C-H$ stretching. The

other modes undergo an almost vertical transition and do not show any change of the excitation with the change of the energy that goes into the vibrational degrees of freedom. The value of ρ $(= e^{-W})$ decreases with the increase of the energy gap between the surfaces. This feature is ascribed to the fact the enlargement of the gap between the surfaces leads to a larger quantum jump between them, a process which is classically forbidden and therefore less probable.

3.6 Influence of the displacements between the two surfaces

The benzene molecule is hexagonal on the ground electronic state and therefore, belongs to the D_{6h} symmetry group. The only modes that can have nonzero displacements under this symmetry are the totally symmetric breathing modes, i.e. q_1 and q_2. If, however, the molecule is distorted on the upper surface, S_2, more modes become totally symmetric and can in principle be displaced. The possibility of an extreme change also in the frequency of these modes is not considered here [39]. How do the displacements, both for a symmetric and for a distorted upper surface, influence the jumping point?

We first take the potentials from section 3.3, implement our maximization procedure and search for jumping points for different displacements of $q_1(C-C)$ and $q_2(C-H)$.

Figure 5 displays the non-zero coordinates of the jumping point with the highest propensity and the value of the Wigner function at this point, versus the displacement of the $C-C$ bond length. From the graph it is easy to see that the main change of the excitation is in the $C-C$ totally symmetric direction. The dependence is linear with a slope of almost 1.1. Changes of the $C-H$ local excitation and of the value of the Wigner function at the jumping point, are small and nonlinear. In figure 6 we display the coordinate of the jumping point with the highest propensity and the value of the Wigner function at this point, versus the displacement of the $C-H$ bond length. Again, the excitation of the displaced mode, here the totally symmetric $C-H$ stretching *normal* mode, is linearly proportional to the displacement (as in a vertical transition). The totally symmetric $C-C$ is not affected at all, while the local $C-H$ stretching mode which is the mode that undergoes the jump is again slightly, nonlinearly, affected. Note that in this framework the normal and local $C-H$ stretching act like almost different directions in space.

It is very likely that a distortion of the conformation of the benzene molecule takes place in the excited state due to a pseudo-Jahn Teller effect. Additional modes that become totally symmetric under the new symmetry can have non-zero displacements. Just as an example, we consider here the case where the molecule remains planar, but belongs to the D_{2h} symmetry group. The modes which will have the most significant distortion will be the modes q_6 and q_8 which correspond to ring deformations(see figure 3). In figure 7 we display the nonzero coordinates of the jumping point with the highest propensity and the value of the Wigner function at this point versus the difference between the angles of the benzene ring, i.e. a nonzero displacement of q_6. Again, we see that the excitation of a displaced mode, here q_6, linearly depends on the displacement. Excitations of the other modes do not significantly change. Figure 8 plots the coordinates of the jumping point with the highest propensity and the value of the Wigner function at this point versus the difference between the $C-C$ bond lengths. This change of the bond lengths induces displacements in q_8 and q_1 and as a result a change in the coordinates of the jumping point. Even for a moderate change in the symmetry a noticeable amount of the energy is transferred to the new modes that are displaced.

- When one direction in phase-space dominates the quantum jump, excitations in other directions are proportional to the displacement, as if in a vertical transition.
- A change of symmetry can strongly influences the jumping point.

3.7 Two anharmonic PES

Having shown in the previous sections the separability in the subspace of $C-H$ stretching modes of the ground surface potential, we study in this subsection the influence of the anharmonicity of the upper surface on the jumping point within the effective one dimensional problem.

Figure 9 displays the one dimensional ground and excited electronic surface potentials in the local mode representation. Relative to the symmetric harmonic potential the anharmonic potential is softened

on its dissociation part and has a sharper slope on its close approach part. Applying a harmonic approximation for both surfaces gives the value of the Wigner function at the jumping point of $W \cong 32$. Taking the ground surface potential to be anharmonic gives the value of $W \cong 17$. Taking into account the anharmonicities of the excited state makes both the wave function and the Wigner function wider on the dissociation side of the potential and narrower on the close approach side. Consequently, the value of the Wigner function at the jumping point $W(q^*, p^*)$ gets a value between the two extremes of $32 \leq W \leq 17$.

For a quantitative analysis of this property and in order to make the calculation with an anharmonic potential that has a closed form expression for the initial Wigner function, we use a Morse approximation for the excited potential surface:

$$V_e(q) = D\left[1 - e^{-\beta(q-q_0)}\right]^2 \tag{31}$$

where: $\beta = \sqrt{2m\omega x_e / \hbar}$ and ω, m, x_e, and $D = \hbar\omega / 4\, x_e$, are the harmonic oscillator frequency, the reduced mass of the mode, the anharmonicity, and the dissociation energy of the excited electronic state. The dissociation energy for the ground electronic state is $D_g = 110.9\,\text{kcal/mol} = 0.1701\,\text{Hartree}$ [40]. Some experimental data, like the acidity of the benzene molecule on the excited electronic state [41], indicate to a difference of less then 10% between the dissociation energy of the excited and ground states. The dashed line in figure 9 is the Morse potential for the above values. From the graph it is obvious that the high order Taylor series anharmonic force field and the Morse potential approximations are very distinct approximations. We prefer therefore to use in this subsection Morse potential for both the ground and excited states.

The wave function of the Morse oscillator is a combination of the associated Laguerre polynomials and the Wigner function is a combination of the modified spherical Bessel function of the third kind (MacDonald function) [42, 43]. The Wigner function of the ground vibrational state is:

$$\rho(q,p) = \frac{2}{\pi\hbar}\frac{x_e^{-2}}{\Gamma(1/x_e - 1)}\, e^{-2\beta(q-q_0)}\, K_{-2ip/\beta\hbar}\left(x_e^{-1}\, e^{-\beta(q-q_0)}\right), \tag{32}$$

where Γ is the Γ function. The order of the MacDonald function that we study is zero because the momentum at the jumping point is zero, $p^* = 0$, and we study $\rho(q, p^*)$. Figure 10b displays some examples of Wigner functions, (with $p = 0$), for the same frequency ω but different anharmonicities x_e. The function is a slightly deformed gaussian where the close approach side of the function decays more rapidly with the increase of the anharmonicity. Figure 10a displays the projection of the jumping point with the highest propensity on the various modes and the value of the Wigner function at this point, versus the anharmonicity parameter x_e of the upper surface, keeping the anharmonicity of the lower surface fixed. The values for W are within the qualitative predicted range discussed above. The only apparent (although small) change of the jumping point with the change of x_e is on the $C - H$ totally symmetric normal mode axis. The deformation of the Wigner function due to the anharmonicity x_e moves the center of the initial wave packet to the dissociation side of the potential. This change of the center of the wave packet leads to an effective positive displacement of the wave packet and the center of the wave packet on the ground electronic surface undergoes an almost vertical transition to a point in space which is displaced with respect to the ground configuration, *although there is no real displacement between the two surfaces.*

Another interesting feature that arises from the reduction of the problem to one dimensional Morse potential regards the direction of the sudden change in the local $C - H$ stretch. One may conclude that the wave packet lands on the ground electronic surface at the close approach side of the potential.

- An increase of the Wigner function at the jumping point is obtained with an increase of the anharmonicity of the lower surface.
- For a fixed anharmonicity of the lower surface, a decrease of the Wigner function at the jumping point is obtained with an increase of the anharmonicity of the upper surface.
- The anharmonicity on the upper surface gives correction to the two extreme approximations of harmonic-harmonic and anharmonic-harmonic potentials.

- Anharmonicity can induce small excitation of non displaced modes due to changes in the center of the initial wavepacket.

3.8 Duschinsky rotation

Consider the impact of a possible Duschinsky rotation which couples q_{14} and q_{15}. Figure 3 displays diagrams of these two modes as they appear on the ground electronic state. Suppose that the new normal modes on the excited state are mixed according to:

$$\begin{pmatrix} q'_{14} \\ q'_{15} \end{pmatrix} = \begin{pmatrix} \cos\beta & \sin\beta \\ -\sin\beta & \cos\beta \end{pmatrix} \begin{pmatrix} q_{14} \\ q_{15} \end{pmatrix} \tag{33}$$

where β is the angle of rotation between the axis. According to Ref. [44], these two modes are coupled in this way on the first excited electronic surface. Here, we consider such a possible coupling for the second excited surface. Other conjectures for other mixing can be studied in a similar way.

The rotation in two dimensions and its influence on the jumping point is demonstrated in figure 11. The contours of the initial Wigner function on the excited electronic surface and the constraint on the lower surface $H_F = E$ are plotted by solid and dashed lines, respectively. The implementation of the Duschinsky rotation is done by rotating the inner ellipse by the angle β. A larger difference between the widths of the Wigner function would increase the effect of the rotation. The effect has to be considered in position as well as in momentum space. However, in our calculations no momentum excitation is found. We first examine the case $\beta = 90^0$, i.e. $q'_{14} = q_{15}$ and $q'_{15} = -q_{14}$ and find a new couple of points with high propensity with a large excitation of q_{14} and small excitations of the totally symmetric $C-C$ and $C-H$ stretching q_1 and q_2. The value of W at these points is 16.8, very close to the value of the points with the highest propensity found without the Duschinsky rotation. The new point that we have found for the extreme rotation is used as an initial point for a local minimum search for different angles of rotation. In figure 12 we display this local minimum which is found in our calculations and the value of the Wigner function at this point versus β, the rotation angle.

A new jumping point with significant propensity develops only for angles of rotation above 65^o. For smaller rotations the point that originates from a rotation exists as a local minimum but has a very high value of W which makes the probability of decaying through this channel negligible.

- Duschinsky effect can cause, in general, a change of the direction of the quantum jump but for the model considered here the angles for rotation needed for this feature to appear are non-physical.

4 Summary and conclusions

The mechanism of surface jumping complements the mechanism of Tully-Preston's surface hopping by extending it to Franck-Condon suppressed transitions. In this paper, the surface jumping approach to nonvertical transitions was developed into a general "ready to use" tool. The formalism was first extended to include forbidden transitions, in particular internal conversion. This results in an additional factor in the FC integrand, a polynomial of the position and momentum of the promoting mode of vibration. In most cases, the influence of the polynomial term on the direction of the jump can be neglected. More generally, the maximization procedure with this additional term is mathematically equivalent to the consideration of a decay not from the ground vibrational state but from a vibrationally excited state. This may worth more studies in the future. A numerical prescription for analyzing the jump was developed for transitions between any general potential energy surfaces, including in particular distorted and anharmonic surfaces. The surface jumping method allows a simple determination of the accepting modes even for systems with a very large dimension.

The surface jumping method for nonvertical transitions was then applied to recognizing accepting modes in a complex model inspired by the $S_2 \rightarrow S_0$ transition in benzene. The transition takes place through non-radiative internal conversion and a large energy of 0.228 eV is released to the vibrational degrees of freedom of the ground S_0 state. We note that experiments have determined the decay rate of vibrationally excited S_2 state to the S_0 electronic state to be at the scales of tens of fs. This supports

the suggestion that the decay occurs via conical intersections between the S_2, S_1, and S_0 surfaces. Here we have ignored the conical intersections and concentrated on a direct quantum jumping process. Future work should address the general question of competing tunneling mechanism, that of surface jumping and that of tunneling through a barrier to get to a conical intersection from an initial vibrationless state. The model incorporates an exact, state of the art, potential surface for the ground electronic state, but a simplistic treatment of the excited electronic state. Dependence on the excited state features is tested by treating as free parameters the energy gap, displacements, and anharmonicities. We observe that for a large energy gap the masses and frequencies become the defining parameters for choosing the accepting mode, while for smaller energy gaps the displacements are more important. Anharmonicities are very important when a competition between degenerate modes occurs. These conclusions are demonstrated by the specific model considered here but apply in general to any weak internal conversion process.

For the model considered here we found that the C-H modes undergo the jump. We showed that the jump takes place in the *local* C-H modes: Since the energy gap between the states is large compared to the vibrational energy scale and the ratio of the harmonic frequencies between the surfaces does not differ very much from one ($0.7 < \omega_k^e \,/\, \omega_k^g < 1.2$), the modes with the largest frequency and smallest reduced mass are the modes that undergo the jump. The *local* $C-H$ in-plane stretching modes take almost all of the electronic energy while all the other modes decays almost vertically.

This finding can be interpreted also within the well known "most probable escape path" principle of the tunnelling phenomena. Due to the fact that in tunnelling the competition is between channels with exponentially small probabilities, there is usually only one channel that dominates. The picture of one mode which undergo quantum jump while the other modes decay vertically was demonstrated in several ways in the paper, e.g., by altering the energy gap between the surfaces, by adding anharmonicities, and by changing the displacement of various modes.

Some of the issues to be considered in the future include a mathematical analysis of different analytic models, transitions from thermal distributions, rotations, and an implementation of the method to other molecules. Application to dissociation, the coupling of the vibrational space of the molecule to additional degrees of freedom of a medium, the dynamics of the molecular wave-packet after the quantum jump between the surfaces takes place, and the calculation of the rate using the phase-space method, could also be studied within this approach.

Acknowledgments

B.S. gratefully acknowledges useful discussions with Prof. Benjamin Scharf. This research was supported by Grants No. 9800460 and No. from the United States - Israel Binational Science Foundation (BSF), Jerusalem, Israel.

References

[1] R.K. Preston, and J. C. Tully, J. Chem. Phys. **54**, 4297 (1971).

[2] M.F. Herman, J. Chem. Phys. **103**, 8081 (1995); **110**, 4141 (1999); **111**, 10427 (1999); and references therein.

[3] M. Ben-Nun, J. Quenneville, and T.J. Martinez, J. Phys. Chem. A **104**, 5161 (2000); M.D. Hack, A.M. Wensmann, D.G. Truhlar, M. Ben-Nun, and T.J. Martinez, J. Chem. Phys. **115**, 1172 (2001); and references therein.

[4] L.D. Landau and E.M. Lifshitz, *Quantum Mechanics* (Pergamon, London, 1958), chapter 7.

[5] E.S. Medvedev, Chem. Phys. **73,** 243 (1982); J. Chem. Phys. **100,** 7192 (1994).

[6] E. E. Nikitin, C. Noda, and R. N. Zare, J. Chem. Phys. **98**, 46-59 (1993); E. E. Nikitin and L. P. Pitaevskii, Phys. Rev. A. **49**, 695-703 (1994); Y. Karni and E. E. Nikitin, J. Chem. Phys. **100**, 2027-2033 (1994); ibid, 8065-8071 (1994); Chemical Physics **191**, 235-246 (1995).

[7] B. Segev and E.J. Heller, J. Chem. Phys. **112**, 4004 (2000).

[8] E.J. Heller and D. Beck, Chem. Phys. Lett. **202**, 350 (1993).

[9] R. Englman, *The Jahn-Teller Effect in Molecules and Crystals* (Wiley Interscience, London-New York, 1972); *Non-Radiative Decay of Ions and Molecules in Solids* (North Holand Pub. Co., Amsterdam, 1979).

[10] J. Jortner, S.A. Rice and R.M. Hochstrasser, Adv. Photochem. **7**, 149 (1969).

[11] V.I. Osherov and E.S. Medvedev, Opt. Spectrosc. (USSR) **67**, 53 (1990).

[12] A. Toniolo and M. Persico, J. Comput. Chem.**22**, 968 (2001), and references within.

[13] E. J. Heller, J. Chem. Phys. **68**, 2066 (1978).

[14] E. J. Heller and R. C. Brown, J. Chem. Phys. **79**, 2226 (1983).

[15] B. Hüpper and B. Eckhardt, Phys. Rev. A. **57**, 1536 (1998).

[16] B. Hüpper and B. Eckhardt, J. Chem. Phys. **110,** 11749 (1999).

[17] The small parameter for the expansion is $s = \left[\hbar/\sqrt{2m\left|\nabla V\right|}\right]^{2/3}/\sigma$. In [16] $s \approx 0.6$ was small enough to assure convergence. Here, the Gaussian on the excited surface has a width of $\sigma = \sqrt{\hbar/m_k\omega_k^e} \approx 0.2$ while the gradient of the ground potential surface at the jumping point is $|V'(q^*)| \approx 1$, $m \approx 2000$, and $s \approx 0.3$. In [16] higher order terms were also calculated, yet this was within a calculation for the rate. Here we calculate propensities, which are controlled by the leading order term in the expansion.

[18] W. H. Press *et al.*, *Numerical Recipes* (Cambridge University Press, Cambridge, 1986) p. 635.

[19] K. Shindo and S. Lipsky, J. Chem. Phys. **45** 2292 (1966).

[20] D.M. Burland and G.W. Robinson, J. Chem. Phys. **51** 4548 (1969).

[21] D.M. Burland, G. Castro, and G.W. Robinson, J. Chem. Phys. **52** 4100 (1970).

[22] C.S. Parmenter and M.W. Schuyler, Chem. Phys. Lett. **6**, 339 (1970).

[23] N. Nakashima and K. Yoshihara, J. Chem. Phys. **79** 2727 (1983).

[24] E. Sekreta and J.P. Reilly, Chem Phys Lett. **149**, 482 (1988).

[25] W.J. Buma, J.H. van der Waals, and M.C. van Hemert, J. Chem. Phys. **93**, 3733 (1990).

[26] W. Radloff, V. Stert, T. Freudenberg, I.V. Hertel, C. Jouvet, C. Dedonder-Lardeux, and D. Solgadi, Chem. Phys. Lett. **281**, 20 (1997).

[27] S.-T. Tsai, C.-K. Lin, Y.T. Lee, and C.-K. Ni, J. Chem. Phys. **113**, 67 (2000).

[28] On conical intersections in general, see for example: D.R. Yarkony, J. Phys. Chem. A **105**, 6277 (2001); and references therein.

[29] I.J. Palmer, I.N. Ragazos, F. Bernardi, M. Olivucci, and M.A. Robb, J. Amer. Chem. Soc. **115** 673 (1993).

[30] B.R. Smith, M.J. Bearpark, M.A. Robb, F. Bernardi, and M. Olivucci, Chem. Phys. Lett. **242** 27 (1995);

[31] E.B. Wilson Jr, J.C. Decius, and P.C. Cross, *Molecular Vibrations and theory of Infrared and Raman Vibrational Spectra* (McGraw-Hill Book Company, New York, 1955), Chapter 10.

[32] L.D. Ziegler and B.S. Hudson, Excited States **5**, 41 (1982).

[33] A. Miani, E. Cane, P. Palmieri, A. Trombetti, and N.C. Handy, J. Chem. Phys. **112**, 248 (2000).

[34] R.J. Sension, R.J. Brudzynsky, S. Li, and B.S. Hudson, J. Chem. Phys. **96**, 2617 (1992).

[35] D. Papoused and M.R. Aliev, *Molecular Vibrational-Rotational Spectra* (Elsevier, Amsterdam, 1982), chapter 23.

[36] B.R. Henry and W. Siebrand, J. Chem. Phys. **49**, 5369 (1968).

[37] See also: L. Halonen, Chem. Phys. Lett. **87**, 221 (1982), and references therein.

[38] S. Rashev, J. Phys. Chem. A **105**, 6499-6505 (2001).

[39] Remarkable changes of the frequencies of q_6 and q_8 (mostly in the triplet state but maybe also in the singlet) were considered for example in B. Scharf, Chem. Phys. Lett. **68**, 242 (1979), and in Ref. [25].

[40] *Handbook of Physical and Chemistry Constants,* edited by S.P. Clarl, Jr. (Spriger, Berlin, 1990).

[41] J.F. Ireland and P.A.H. Wyatt, Adv. Phys. Org. Chem. **12**, 131 (1976).

[42] H.W. Lee, Phys Rep. **259**, 147 (1995).

[43] A. Frank, A.L. Rivera, and K.B. Wolf, Phys. Rev. A **61**, 4102 (2000).

[44] G. Fischer, *Vibronic Coupling* (Academic Press, London, 1984).

q_1	q_2	q_7	q_{13}	q_{20}	q_{7a}	q_{20a}	W
0.08	*-0.31*	*-0.44*	*-0.31*	*-0.44*	*0*	*0*	*17.00*
0.08	*-0.31*	*-0.44*	*0.31*	*0.44*	*0*	*0*	*17.00*
0.08	*-0.32*	*0.22*	*0.31*	*-0.22*	*-0.38*	*-0.38*	*17.02*
0.08	*-0.32*	*0.22*	*-0.31*	*0.22*	*-0.38*	*0.38*	*17.02*
0.08	*-0.32*	*0.22*	*-0.31*	*0.22*	*0.38*	*-0.38*	*17.02*
0.08	*-0.32*	*0.22*	*0.31*	*-0.22*	*0.38*	*0.38*	*17.02*

Table 1: Local maximum or jumping points obtained for the $S_2 \rightarrow S_0$ transition using the potential of section 3.3. The points are given in the normal mode representation

s_1	s_2	s_3	s_4	s_5	s_6	W	
-0.76	0.	0.	0.	0.	0.	17.00	
0.	0.	0.	-0.76	0.	0.	17.00	
0.	-0.76	0.	0.	0.	0.	17.02	
0.	0.	-0.76	0.	0.	0.	17.02	
0.	0.	0.	0.	-0.76	0.	17.02	
0.	0.	0.	0.	0.	-0.76	17.02	

Table 2: The points of table 1 in the local mode representation.

Figure 1: Two kinds of transitions: vertical and non-vertical. (a) Radiationless vertical transition between crossing surfaces. The transition takes place by continuous changes of the coordinates and via the point of crossing between the surfaces. (b) Radiationless non-vertical transition for nested surfaces - surface jumping. The transfer of the energy must occur by a sudden change of position or momentum. The direction of the jump is not obvious a priory. Our purpose is to predict this direction. (c) Radiative vertical transition, equivalent to the radiationless case (a): most of the energy goes to the emitted photon. The transition takes place by continuous changes of the coordinates and via the point of crossing between the dressed initial surface and the final accepting energy surface. (d) Radiative non-vertical transition, equivalent to the radiationless case (b): such transitions occur in the blue wing of an absorption band, where some of the energy of the absorbed photon is transferred into vibrational energy via surface jumping.

Figure 2: Geometric representation of the method for finding the direction of the quantum jump in two dimensions (Q_1, Q_2). The outer dashed ellipse represents the constraint $H_F(Q_1, Q_2) = E$. The inner solid ellipses represents the contours of the Wigner function on the upper surface. (a) The case of strong maximum. The value of the Wigner function decreases rapidly with the distance from the jumping point. The jumping point is well defined. (b) Weak maximum - the jumping point is not well defined.

Figure 3: The $C-H$ in-plane stretching normal modes. q_2 $(a_{1g})$and $q_{13}(b_{1u})$ are two non-degenerate modes. q_2 is the totally symmetric $C-H$ stretching. $q_7(e_{2g})$ and $q_{20}(e_{1u})$ are two degenerate modes. q_6 and q_8 which correspond to ring deformations are involved in a possible pseudo Jahn Teller effect on S_2. Both modes belong to the e_{2g} representation for the D_{6h} symmetry and to the a_g representation of the D_{2h} symmetry. q_{14} and q_{15} are two normal modes considered here to be involved in a possible Duschinsky rotation. Both modes belong to the b_{2u} representation, q_{14} is a ring stretching mode, and q_{15} is a $C-H$ bending mode.

Figure 4: Results of the calculation for the $S_2 \rightarrow S_0$ transition taking the potentials of section 3.3 with the energy gap between the electronic surfaces considered as a free parameter. The coordinate and the value of the Wigner function at the jumping point are plotted vs. the energy gap between the surfaces. The value of the Wigner function at the jumping point exponentially depends on the energy gap.

Figure 5: Same as figure 4 with the displacement of the $C-C$ totally symmetric mode considered as a free parameter. The coordinates and the value of the Wigner function at the jumping point are plotted vs. the $C-C$ displacement between the two surfaces. The excitations of the local $C-H$ and totally symmetric $C-C$ stretching and the value of the Wigner function $-\ln\rho = W$ at the jumping point are displayed in solid, dashed, and close-circles lines, respectively. The excitation of the displaced mode linearly depends on its displacement.

Figure 6: Same as figure 4 with the displacement of the $C-H$ totally symmetric mode considered as a free parameter. The coordinate and the value of the Wigner function at the jumping point are plotted vs. the $C-H$ displacement between the two surfaces.

Figure 7: Results of the calculation for the $S_2 \rightarrow S_0$ transition taking the potentials of section 3.3 and including a pseudo-JT deformation of the benzene angles. The coordinate and the value of the Wigner function at the jumping point are plotted vs. the difference between the angles of the benzene molecule. The excitations of the local $C-H$, totally symmetric $C-C$ stretching, q_6 and the value of the Wigner function $-\ln\rho = W$ at the jumping point are displayed in solid, dotted, dashed and close-circles lines, respectively.

Figure 8: Same as figure 7 but with a pseudo-JT deformation of the $C-C$ bond lengths of the benzene.

Figure 9: Local $C-H$ stretching potentials. The harmonic, anharmonic, and Morse potentials for the local $C-H$ stretching of the S_0 and S_2 electronic states are shown in solid, dotted-dashed, and dashed lines, respectively. The anharmonicity of the upper surface is plotted here as if equal for the two electronic states, but is considered as a free parameter in the calculations.

Figure 10: (a) Results of the calculation for the $S_2 \rightarrow S_0$ transition taking the Morse potentials for both surfaces. The coordinate and the value of the Wigner function at the jumping point are plotted vs. the anharmonicity x_e of the upper electronic surface. The excitations of the local $C-H$, totally symmetric $C-C$ stretching, normal $C-H$ stretching and the value of the Wigner function $-\ln\rho = W$ at the jumping point are displayed in solid, dotted, dashed and close-circles lines. (b) Wigner function for the Morse oscillator with $\omega = 3212\ cm^{-1}$ and different anharmonicities x_e.

Figure 11: Geometric demonstration of the Duschinsky mode rotation in two dimensions. The solid lines represent the contours of the Wigner initial function on the excited electronic surface. The outer dashed ellipse represents the constraint surface for the lower surface $H_F = E$. Implementation of the Duschinsky rotation is done by rotating the inner ellipse by β.

Figure 12: Results of the calculation for the $S_2 \rightarrow S_0$ transition taking the potentials of section 3.3 and including a Duschinsky mode rotation between q_{14} and q_{15}. The coordinates and the value of the Wigner function at the jumping point are plotted vs. the rotation angle β. The excitations of the local $C - H$, totally symmetric $C - C$ stretching, q_{14}, q_{15} and the value of the Wigner function $-\ln \rho = W$ at the jumping point are displayed in solid, dashed, dotted, dotted-dashed and close-circles lines, respectively.

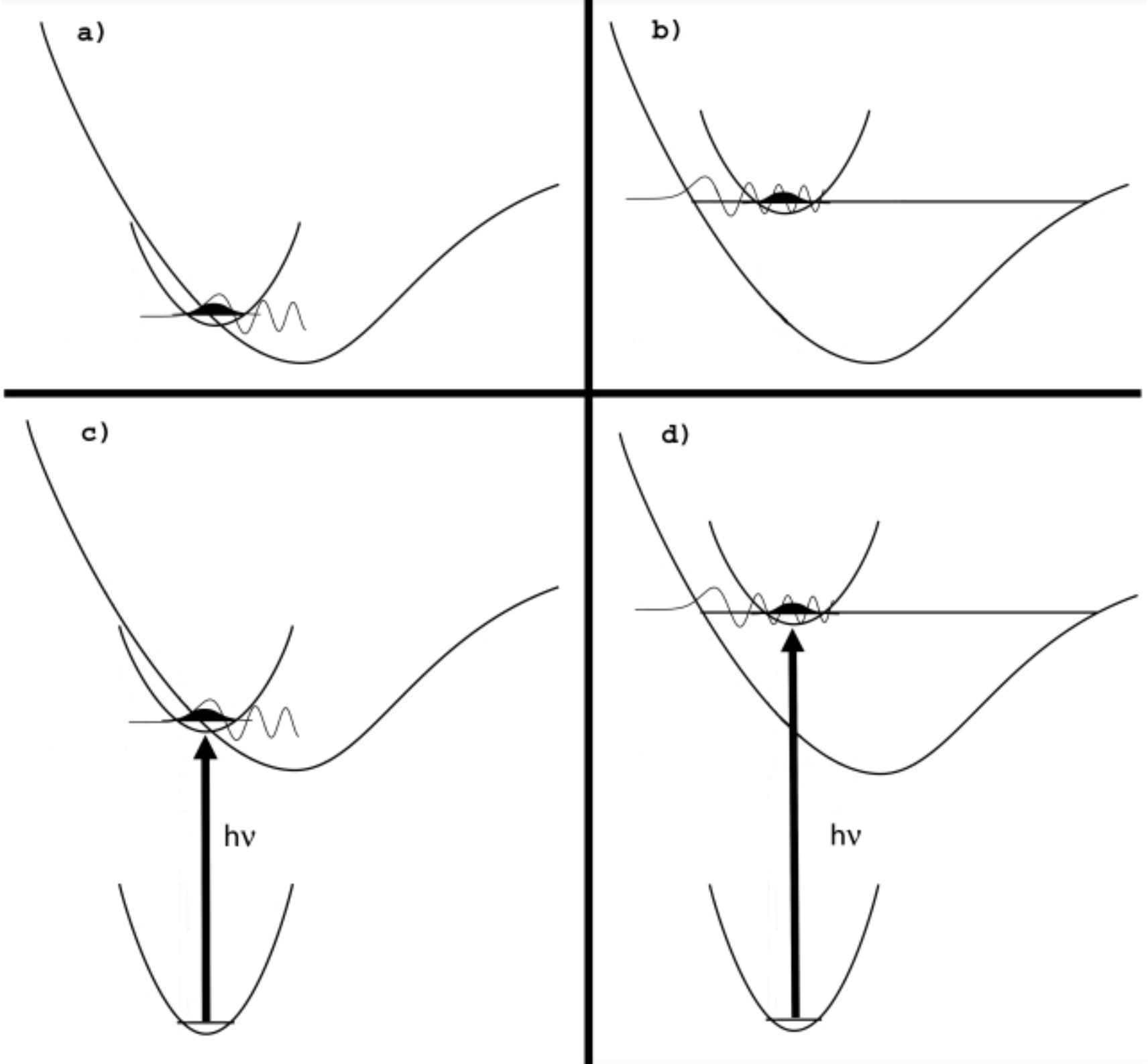
a)
b)
c)
hν
d)
hν

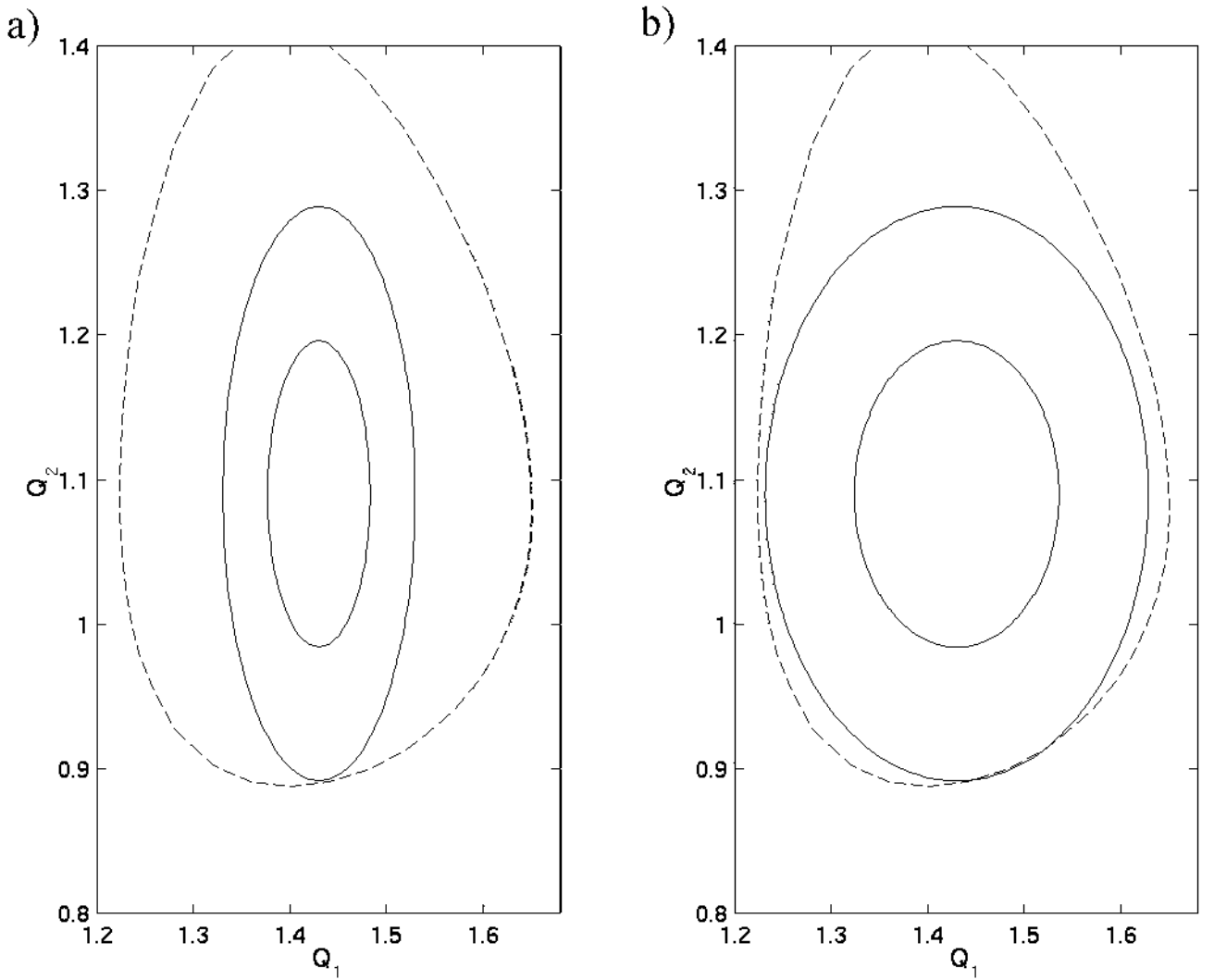
a)
b)
1.4
1.3
1.2
1.1
1
0.9
0.8
Q_2
1.2
1.3
1.4
1.5
1.6
Q_1

Non-degenerate

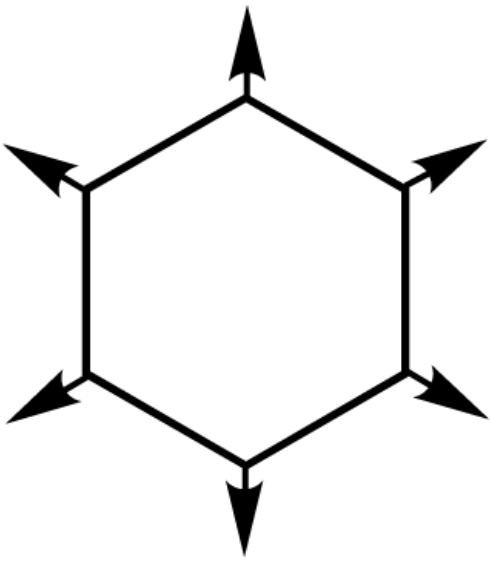

q_2

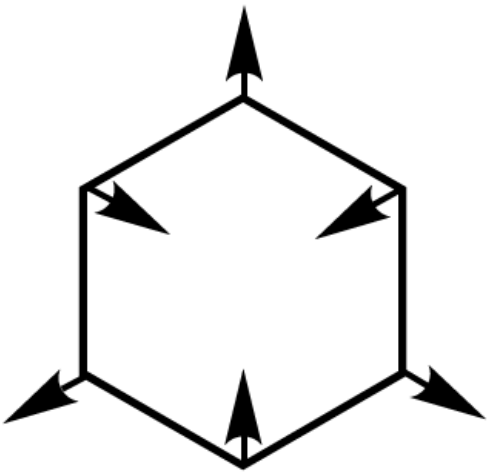

q_{13}

Degenerate

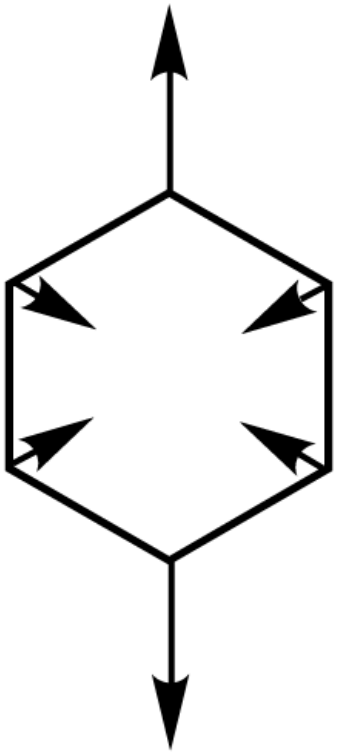

q_7

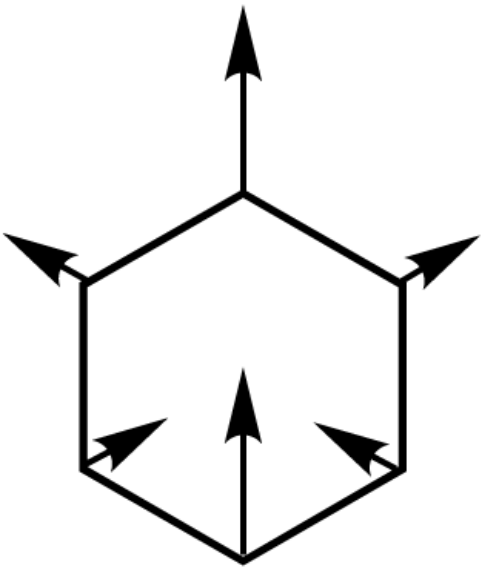

q_{20}

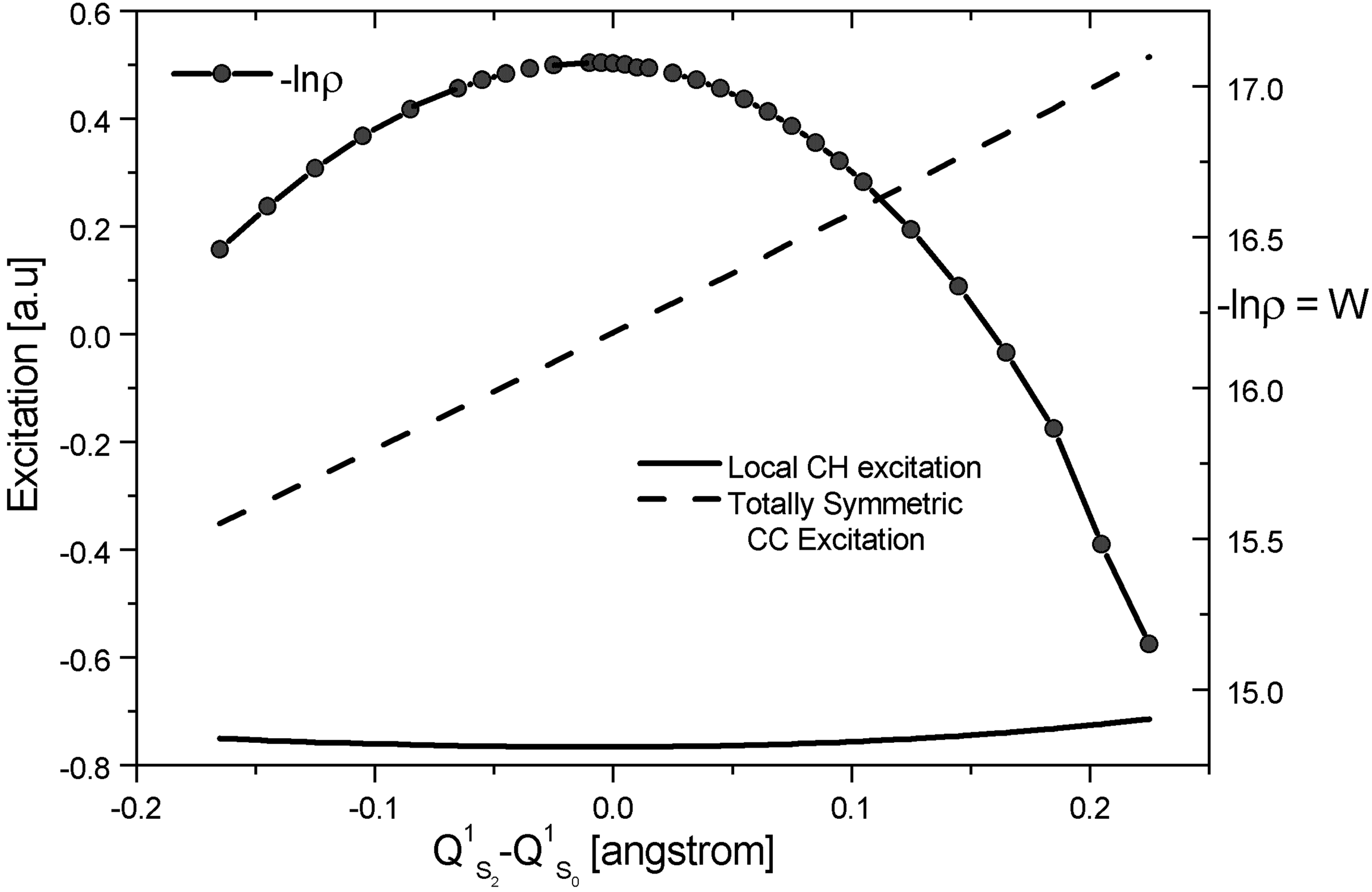
0.6
0.4
0.2
0.0
-0.2
-0.4
-0.6
-0.8
Excitation [a.u]
-lnρ
17.0
16.5
16.0
15.5
15.0
-lnρ = W
Local CH excitation
Totally Symmetric
CC Excitation
-0.2
-0.1
0.0
0.1
0.2
Q1S2-Q1S0 [angstrom]

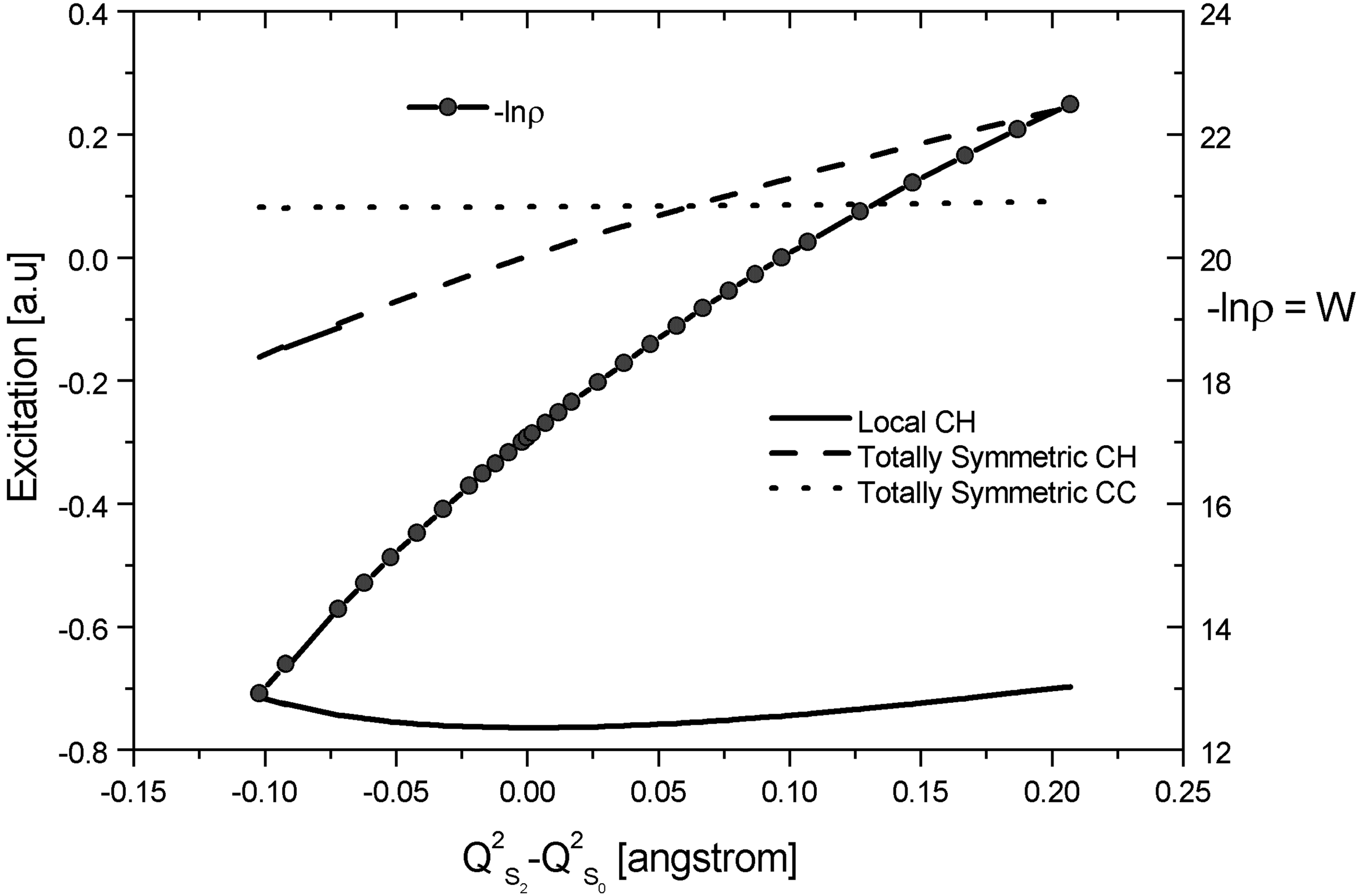
-lnρ
Local CH
Totally Symmetric CH
Totally Symmetric CC
Excitation [a.u]
-lnρ = W
$Q^2_{S_2}-Q^2_{S_0}$ [angstrom]
0.4
0.2
0.0
-0.2
-0.4
-0.6
-0.8
24
22
20
18
16
14
12
-0.15
-0.10
-0.05
0.00
0.05
0.10
0.15
0.20
0.25

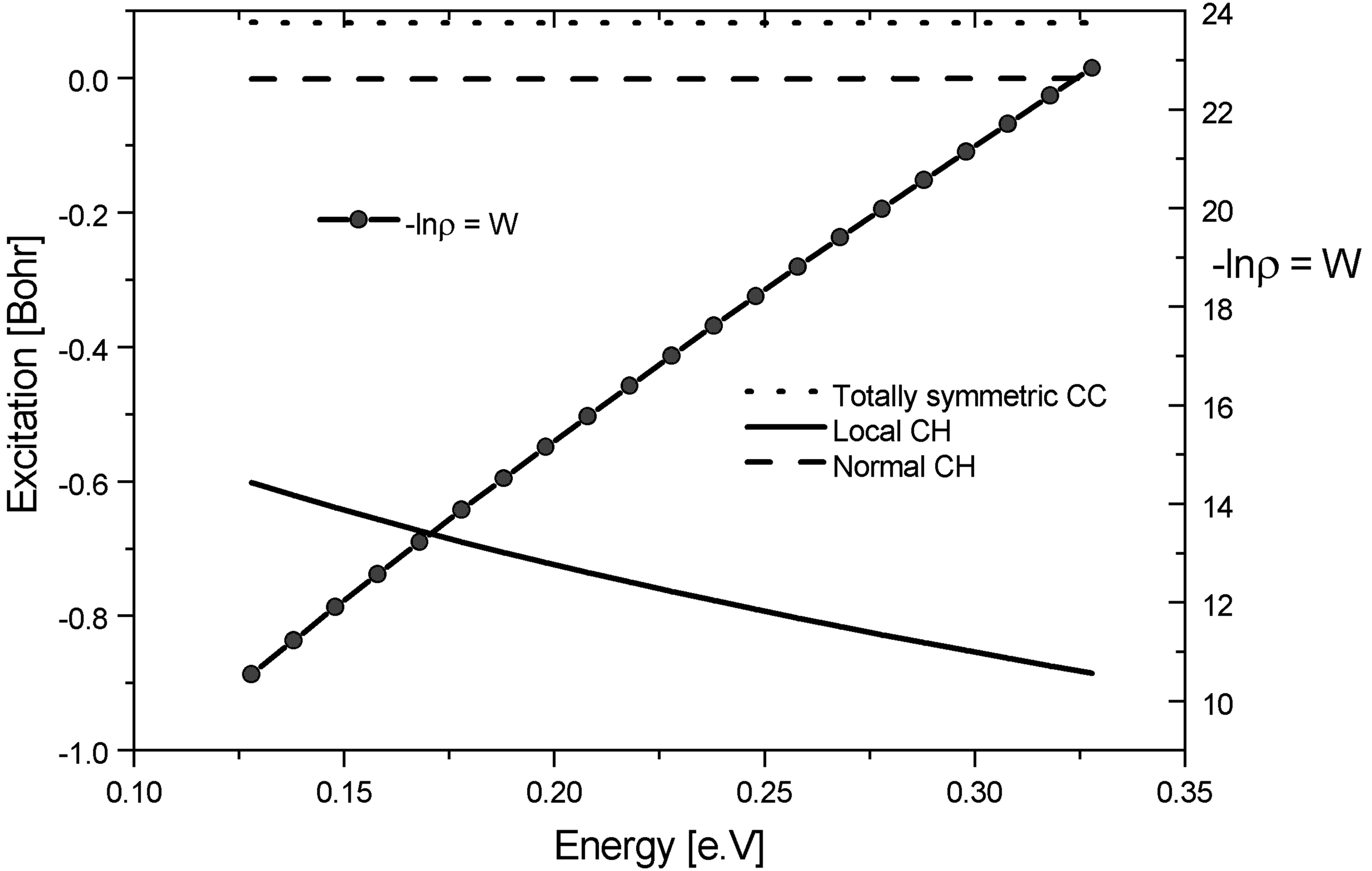
0.0
-0.2
-0.4
-0.6
-0.8
-1.0
Excitation [Bohr]
0.10
0.15
0.20
0.25
0.30
0.35
Energy [e.V]
24
22
20
18
16
14
12
10
-lnρ = W
-lnρ = W
Totally symmetric CC
Local CH
Normal CH

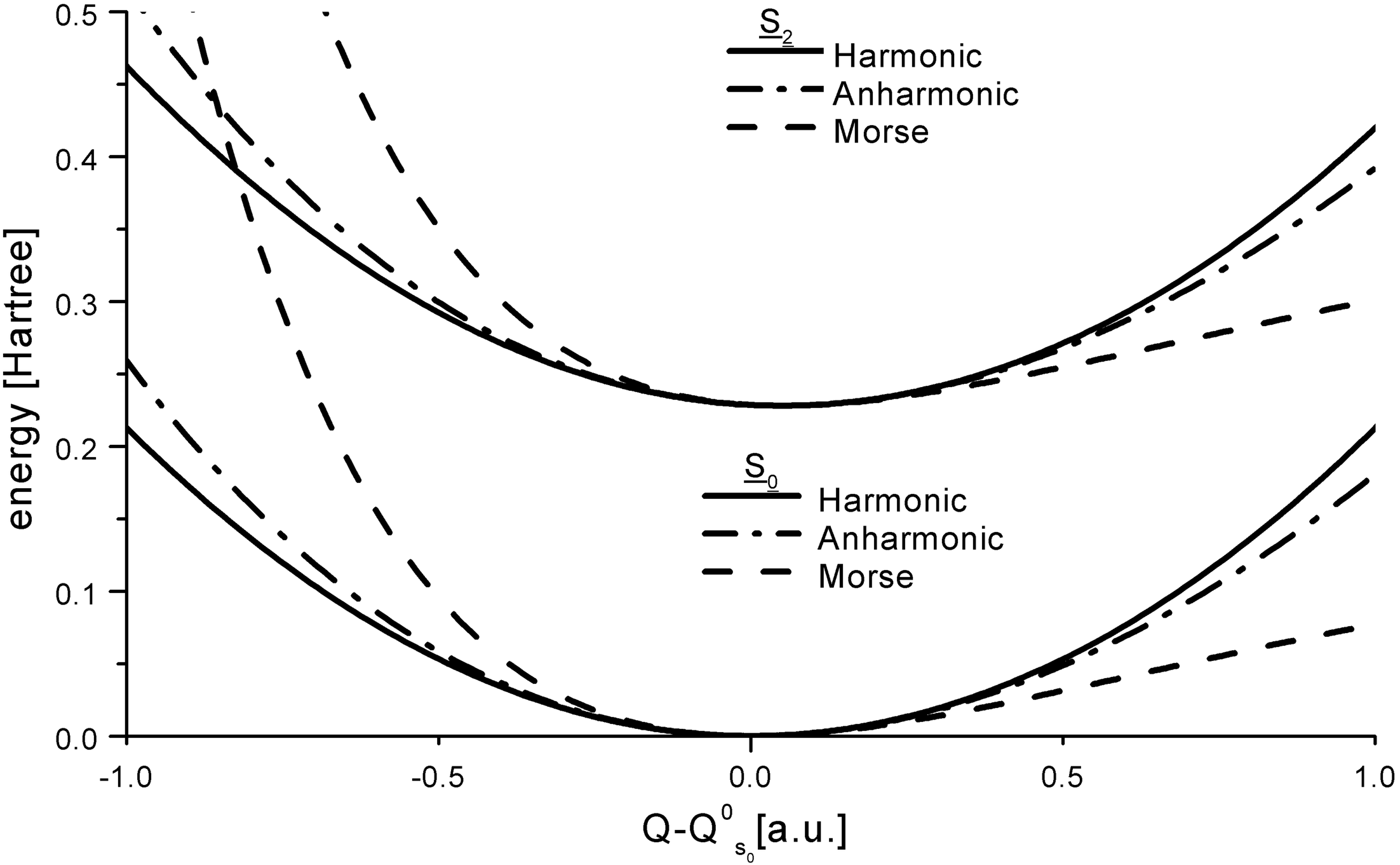
0.5
0.4
0.3
0.2
0.1
0.0
energy [Hartree]
-1.0
-0.5
0.0
0.5
1.0
Q-Q$^0_{s_0}$[a.u.]
S$_2$
Harmonic
Anharmonic
Morse
S$_0$
Harmonic
Anharmonic
Morse

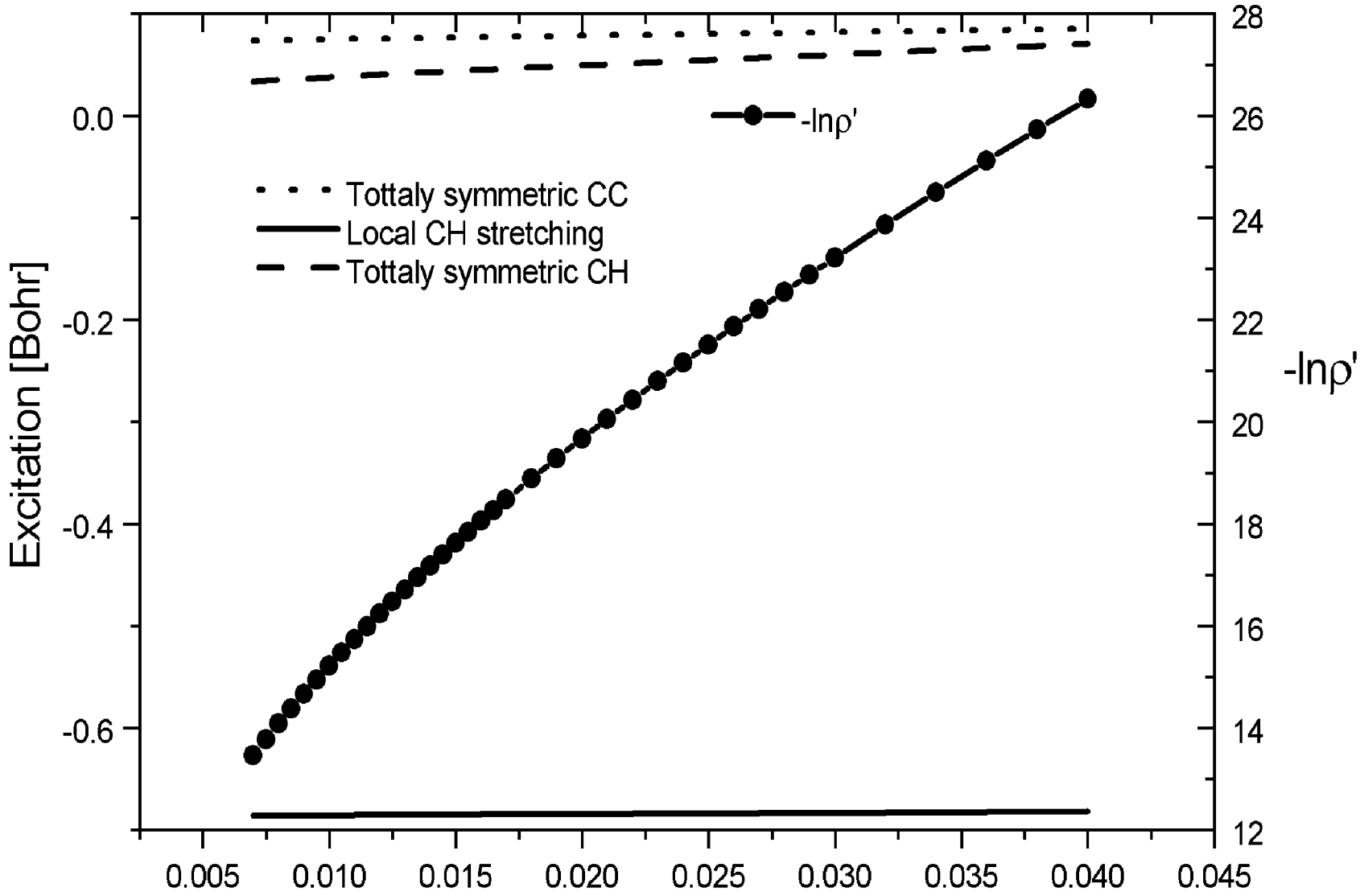
Excitation [Bohr]
0.0
-0.2
-0.4
-0.6
28
26
24
22
20
18
16
14
12
-lnρ'
-lnρ'
Tottaly symmetric CC
Local CH stretching
Tottaly symmetric CH
0.005
0.010
0.015
0.020
0.025
0.030
0.035
0.040
0.045

x_e

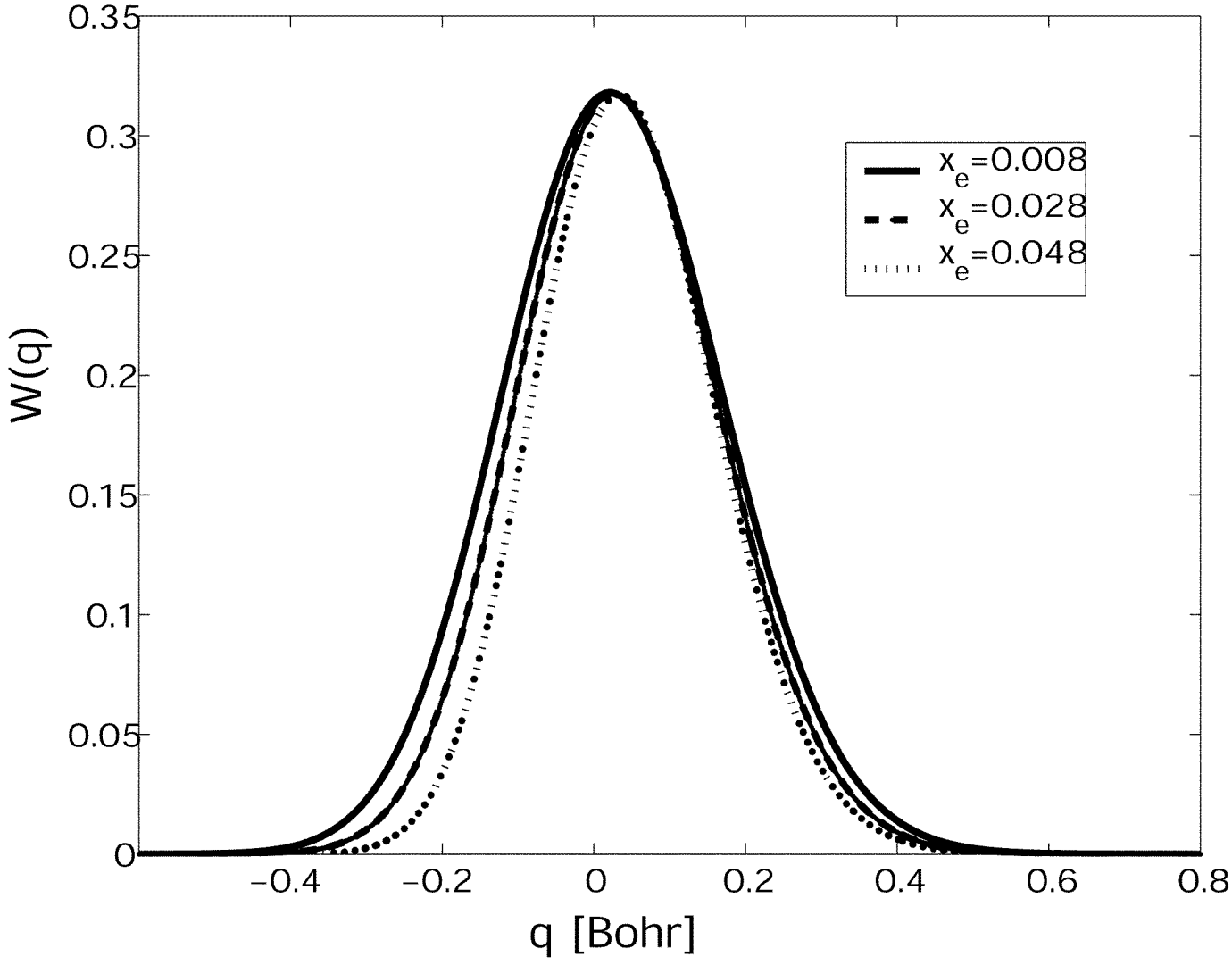
W(q)
0.35
0.3
0.25
0.2
0.15
0.1
0.05
0
x_e=0.008
x_e=0.028
x_e=0.048
−0.4
−0.2
0
0.2
0.4
0.6
0.8
q [Bohr]

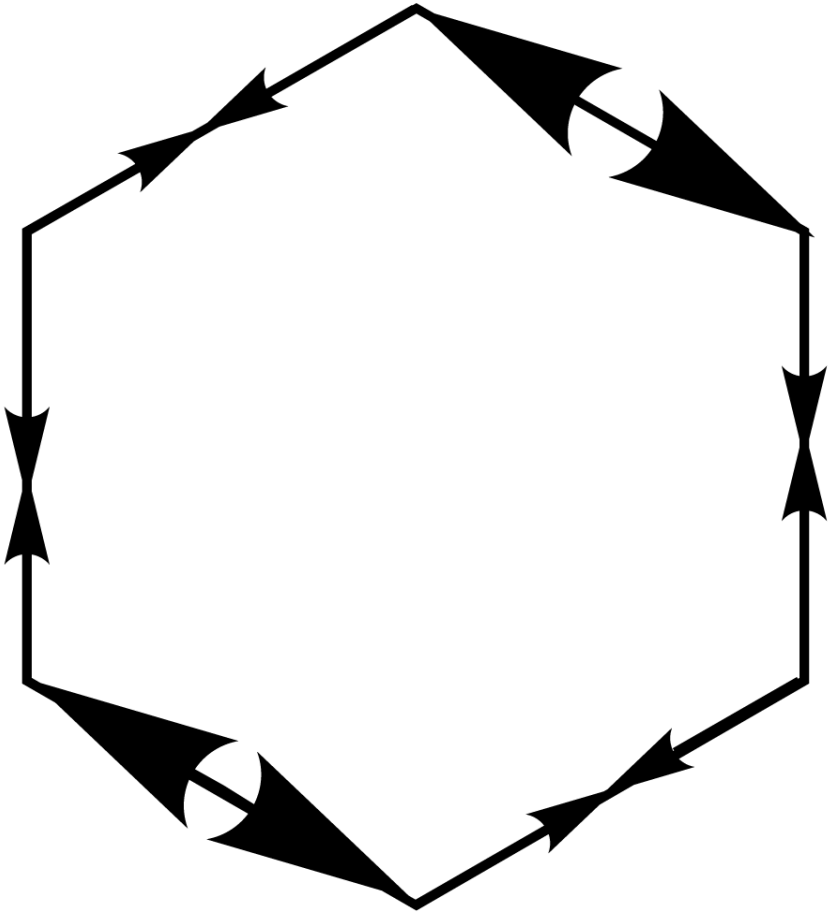

q_8

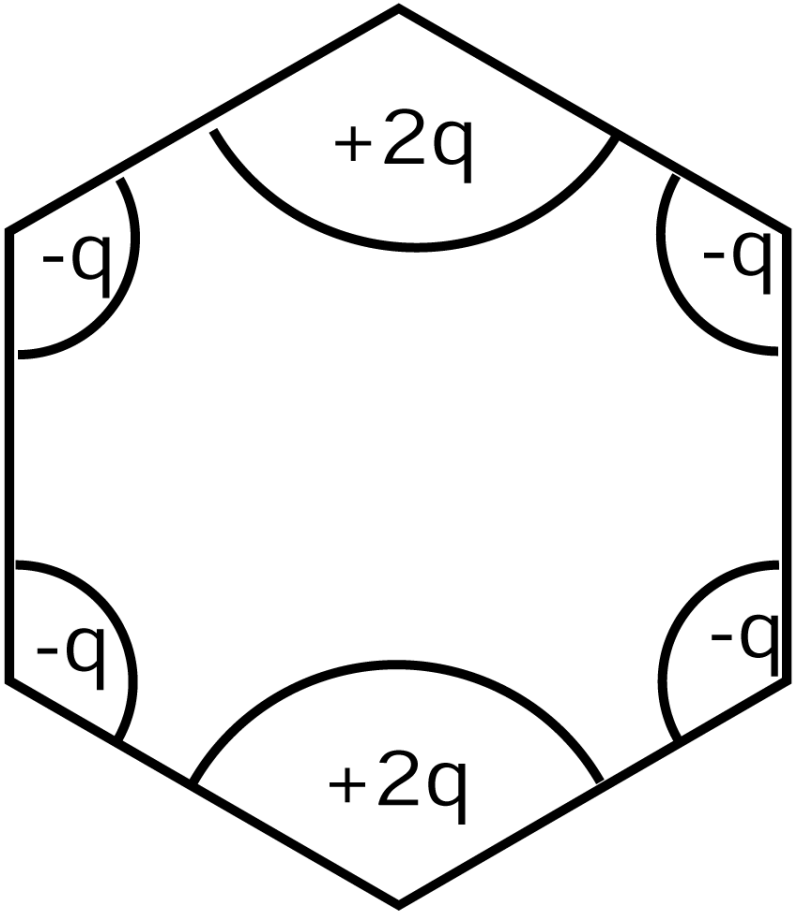

q_6

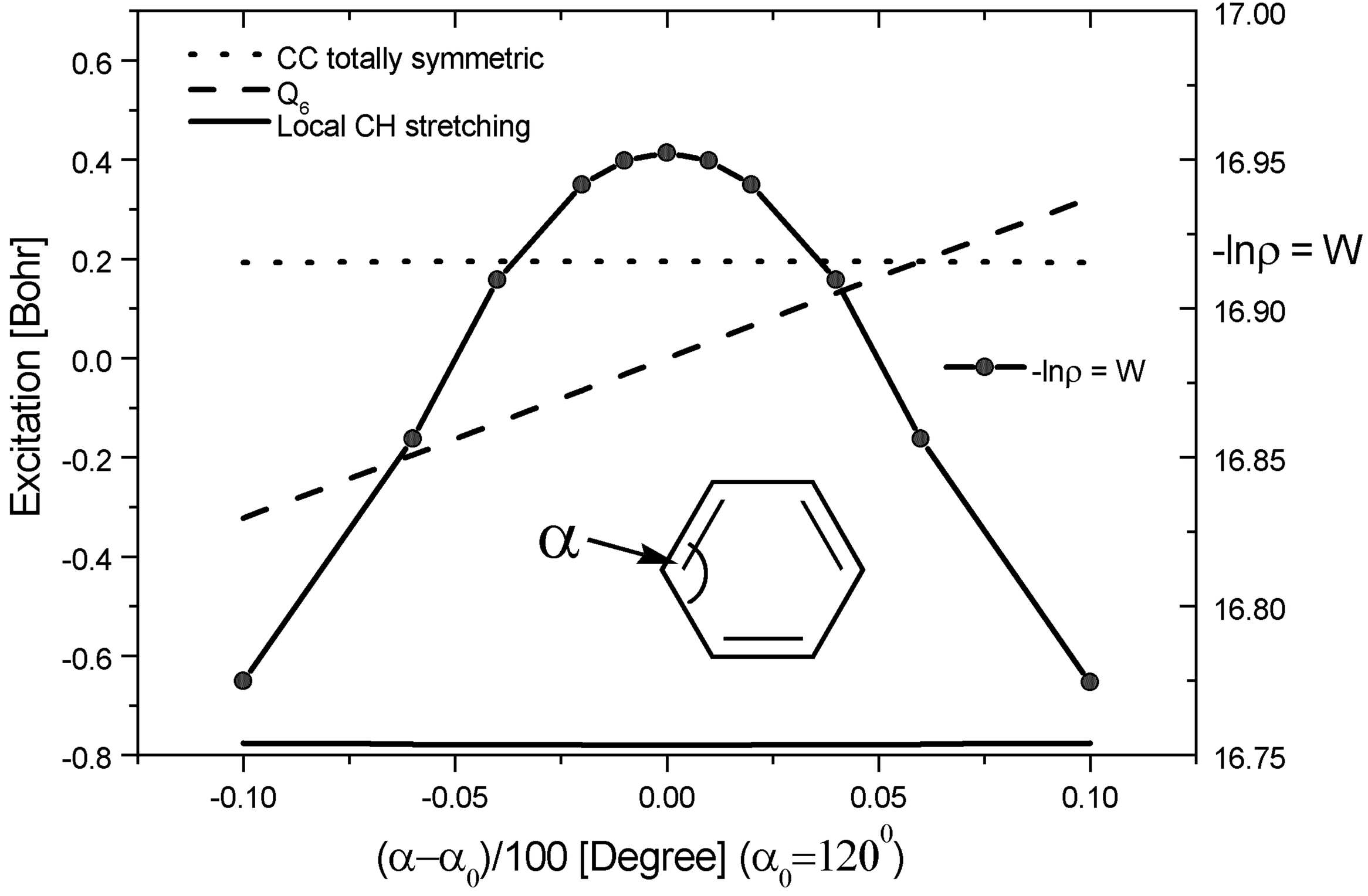
CC totally symmetric
Q_6
Local CH stretching
-lnρ = W
α
Excitation [Bohr]
0.6
0.4
0.2
0.0
-0.2
-0.4
-0.6
-0.8
17.00
16.95
16.90
16.85
16.80
16.75
-lnρ = W
-0.10
-0.05
0.00
0.05
0.10
$(\alpha-\alpha_0)/100$ [Degree] ($\alpha_0=120^0$)

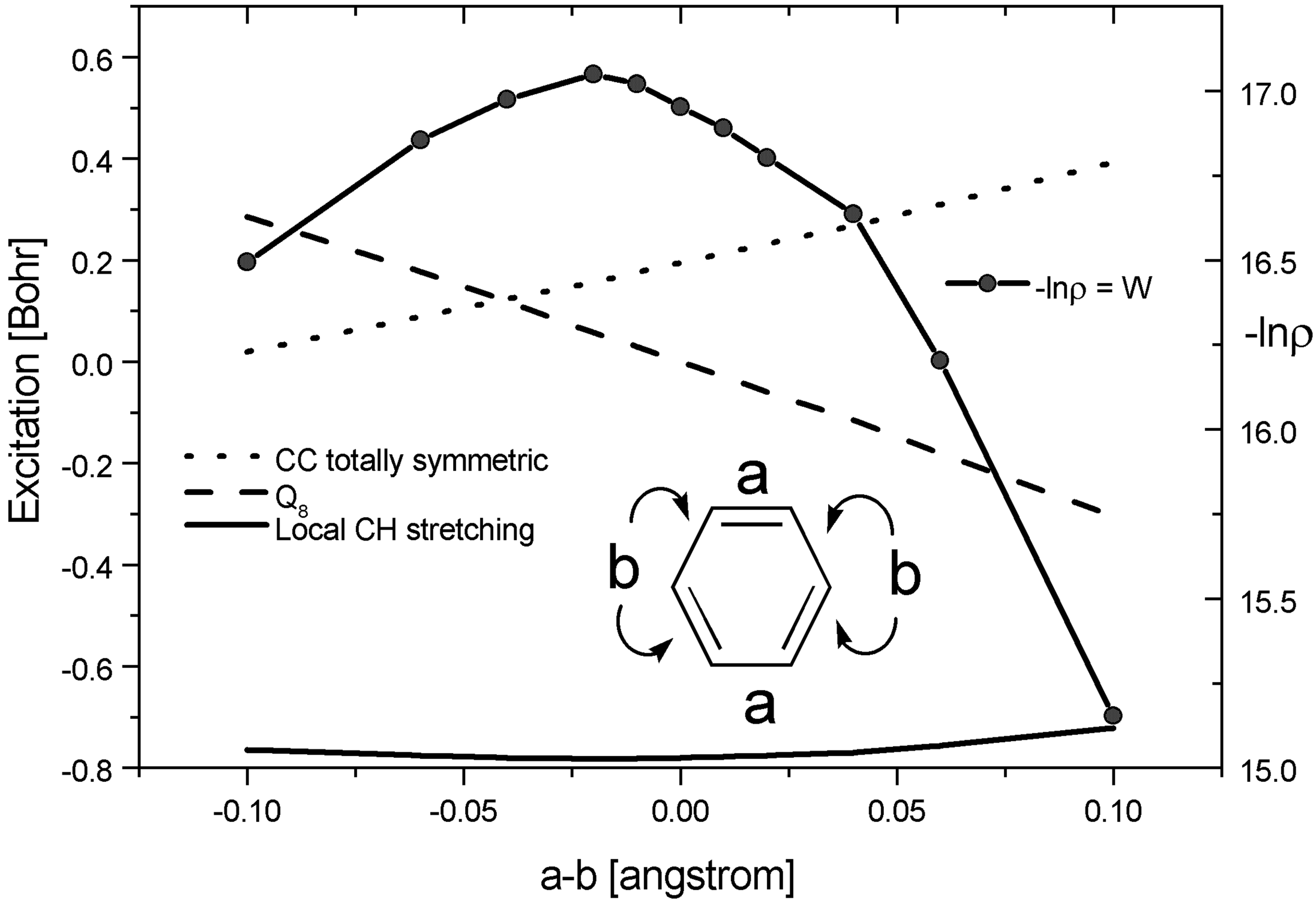
0.6
0.4
0.2
0.0
-0.2
-0.4
-0.6
-0.8
Excitation [Bohr]
17.0
16.5
16.0
15.5
15.0
-lnρ = W
-0.10
-0.05
0.00
0.05
0.10
a-b [angstrom]
CC totally symmetric
Q8
Local CH stretching
a
b
b
a

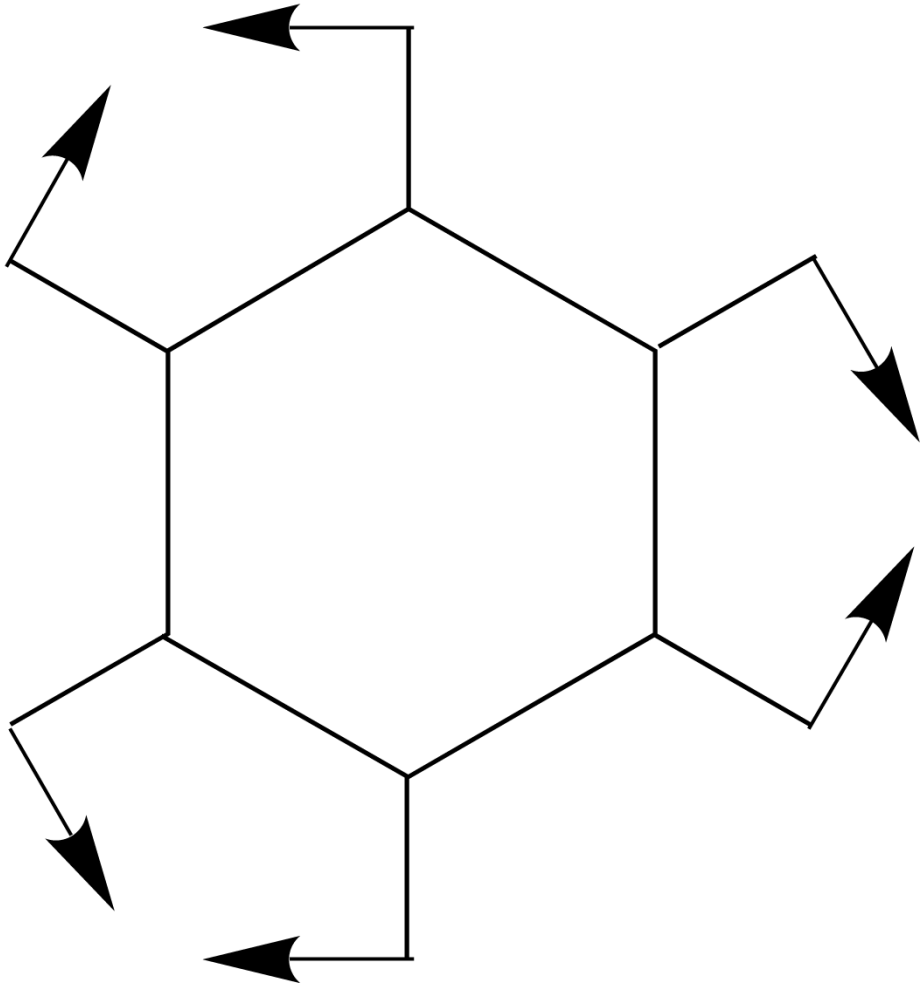

q_{14}

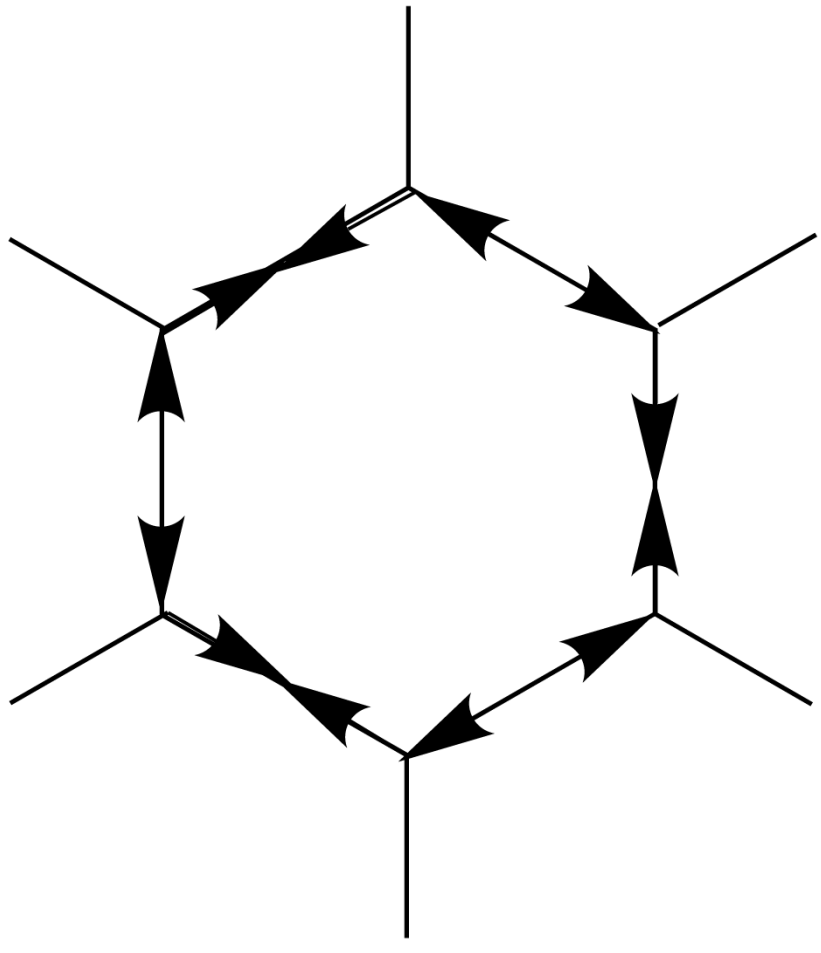

q_{15}

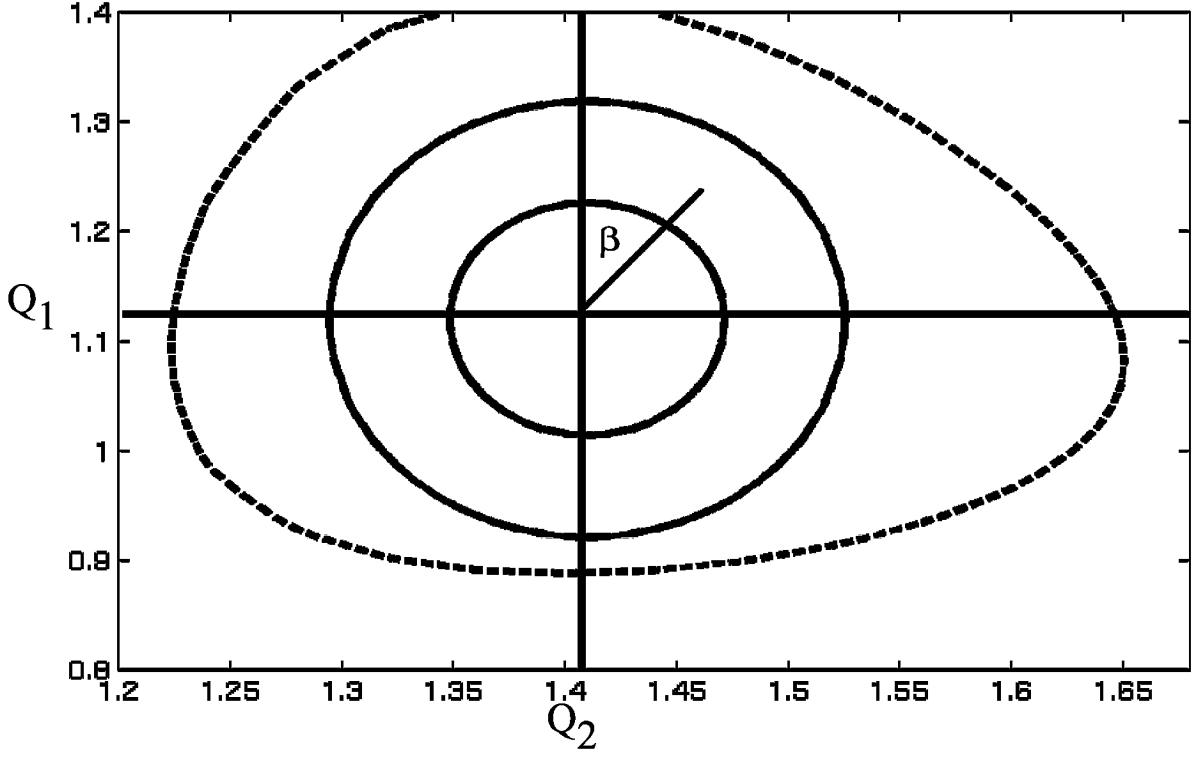
1.4
1.3
1.2
1.1
1
0.9
0.8
Q_1
β
1.2
1.25
1.3
1.35
1.4
1.45
1.5
1.55
1.6
1.65
Q_2

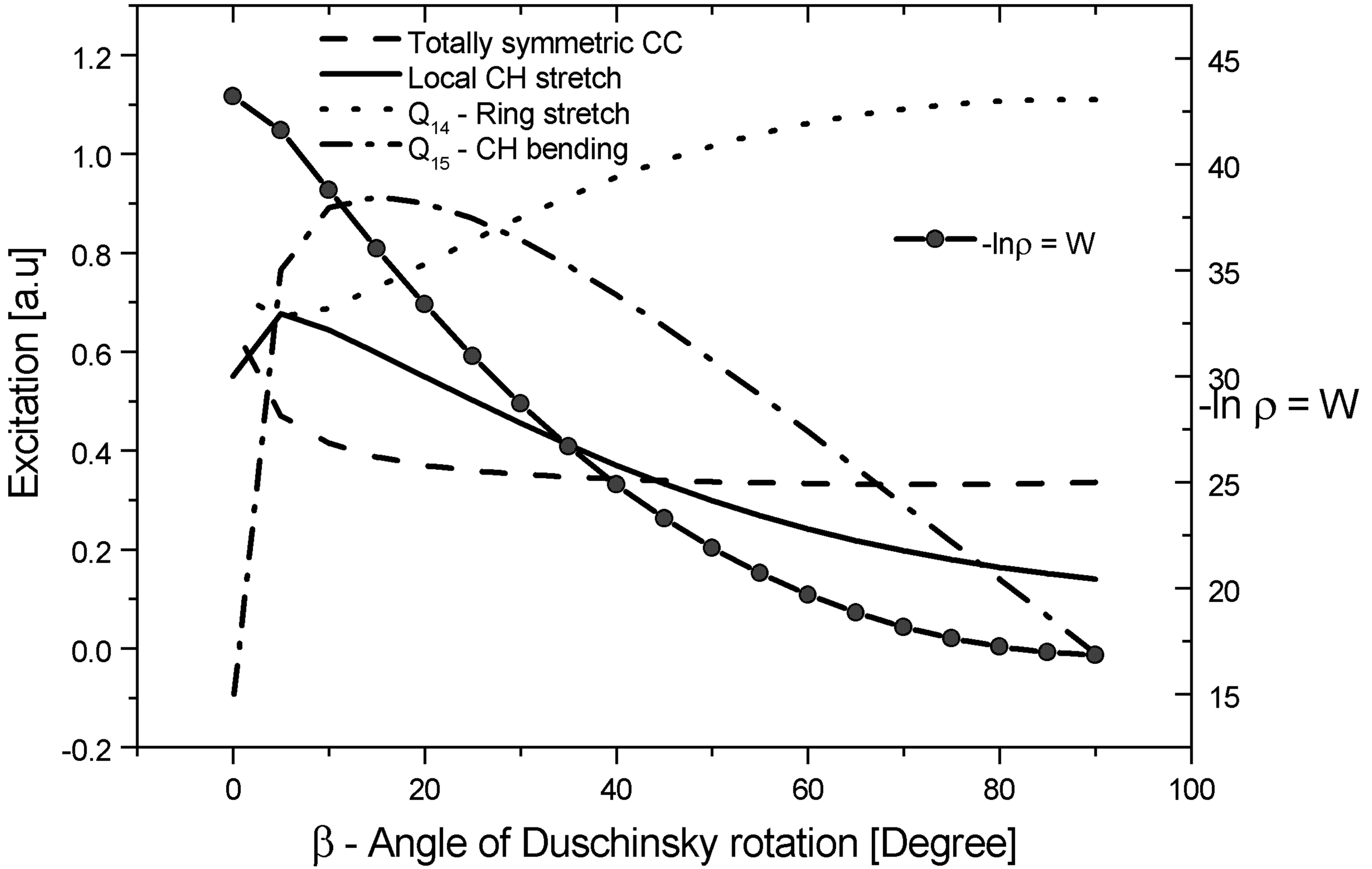
Totally symmetric CC
Local CH stretch
Q14 - Ring stretch
Q15 - CH bending
-lnρ = W
Excitation [a.u]
-ln ρ = W
β - Angle of Duschinsky rotation [Degree]
1.2
1.0
0.8
0.6
0.4
0.2
0.0
-0.2
45
40
35
30
25
20
15
0
20
40
60
80
100